Study on nuclear localization of myosin regulatory light chain in response to substrate stiffness

基質の硬さに依存したミオシン調節軽鎖の核局在についての研究

Katsuya Onishi

March 2024

Doctoral Dissertation

Division of Soft Matter
Graduate School of Life Science
Hokkaido University

Table of contents

Chapter 1

General Introduction

1-1 Cell response for substrate stiffness

The intricate interaction between cells and their surrounding extracellular matrix (ECM) significantly influences cellular behavior, dictating their response to physical properties determined by ECM structure and composition[1,2] (Fig. 1.1). Each tissue meticulously regulates its ECM's structure and composition to optimize cellular function[3]. Appropriate tissue stiffness regulates stem cell differentiation and morphogenesis[4-6], whereas an abnormal increase in ECM stiffness triggers aberrant cellular behaviors associated with aging, cancer progression, fibrosis, and cardiovascular ailments[7]. In fact, it has been reported that fibrosis lung and liver tissue stiffness become 25-100 kPa, while the normal tissue stiffness is 0.5-1 kPa (Fig. 1.2). Particularly, elevated substrate stiffness has been correlated with the induction of cancerous traits in vitro, notably enhancing cell proliferation [8] and epithelial–mesenchymal transition[9] In addition, tissue stiffening exacerbates the disease such as cancer progression and dysfunction of that organ. (Fig. 1.3). Thus, Elucidating cellular responses to substrate stiffness is pivotal in unraveling physiological homeostasis and disease mechanisms. Traditionally, tumor stiffness serves as a diagnostic marker and, more recently, as a prognostic factor[10].

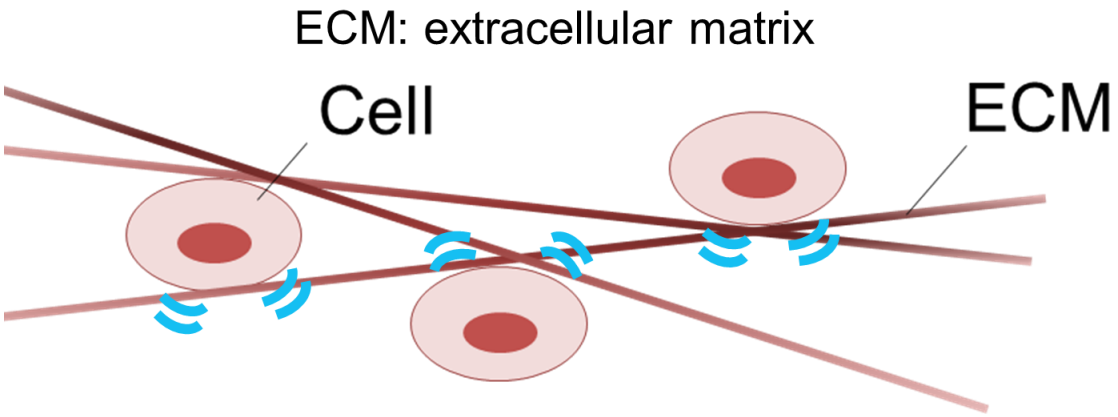

Fig. 1.1 Cells sense stiffness of substrate such as ECM.

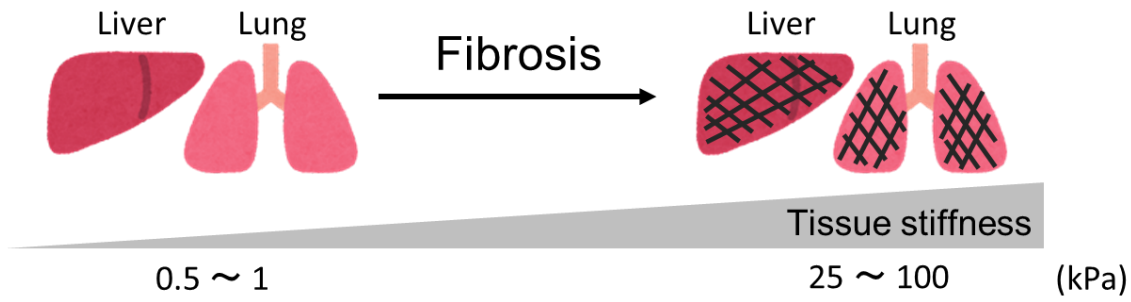

Fig. 1.2 Tissue fibrosis promote tissue stiffening.

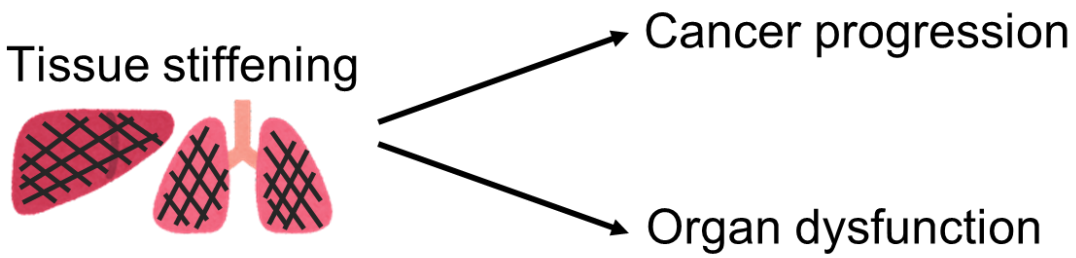

Fig. 1.3 Tissue stiffening exacerbates the disease.

1-2 Mechanotransduction

Cell responses to mechanical cues involve a crucial mechanism known as mechanotransduction, where mechanical stimuli get translated into biochemical signals.[11]. Cellular response to stiffness is mediated by the nuclear translocation of stiffness-responsive transcription factors and the regulation of gene expression (Fig. 1.4). Transcription factors such as β-catenin[12], myocardin related transcription factor-A (MRTF-A)[13], nuclear factor-κB (Nf-κB)[13], SNAIL1[14], twist family bHLH transcription factor 1 (TWIST1)[9], and Yes-associated protein (YAP)[15] respond to substrate stiffness by relocating to the nucleus. This shift in matrix stiffness significantly influences cancer progression by controlling these transcription factors[16]. Despite this knowledge, there's still much we don't understand about how cells specifically react to substrate stiffness using these known transcription factors.

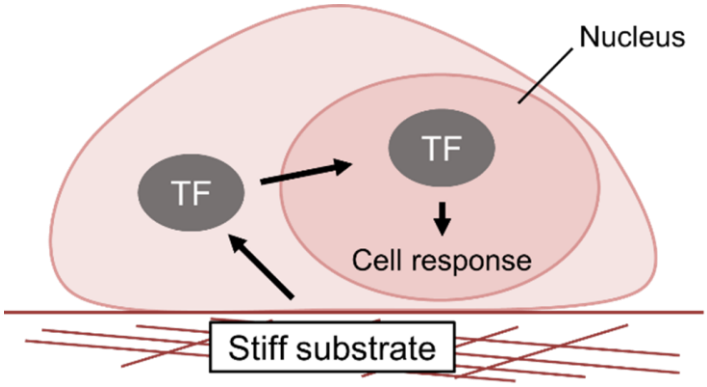

Fig. 1.4 the mechanism that cells response to substrate stiffness

Some transcription factors (TFs) respond to stiffness and localized to the nucleus. Once in the nucleus, these TFs triggered by substrate stiffness play a crucial role in prompting cellular responses by modulating gene expression.

Chapter 2

Materials and Methods

2-1 Reagent

Product	Dilution rate	Source	Identifier
Antibodies for Immunofluorescent staining			
Rabbit anti-MRLC	1:200	CST	3672
Rabbit anti-pMRLC (ser19)	1:200	CST	3671
Rabbit anti-pMRLC (Thr18/ser19)	1:150	CST	3674
Rabbit anti-ZIPK	1:200	abcam	ab210528
Goat anti-Rabbit IgG Alexa Fluor 488	1:200	Invitrogen	A28175
Antibodies for western blotting			
Rabbit anti-Caspase 3	1:1,000	CST	9662
Mouse anti-GAPDH	1:100,000	Invitrogen	AM4300
Mouse anti-Lamin A/C	1:10,000	CST	4777
Rabbit anti-MAFB	1:5,000	CST	30919
Rabbit anti-MRLC	1:1,000	CST	3672
Rabbit anti-pMRLC (ser19)	1:1,000	CST	3671
Rabbit anti-pMRLC (Thr18/ser19)	1:1,000	CST	3674
Mouse anti-α-Tubulin	1:10,000	Sigma	T9026
Rabbit anti-ZIPK	1:5,000	Sigma	Z0134
Goat anti-Rabbit IgG, HRP linked	same dilution rate as the primary antibody	CST	7074
Goat anti-Mouse IgG, HRP linked	same dilution rate as the primary antibody	CST	7076
Phalloidins for fluorescent observation			
Alexa Fluor 546 Phalloidin	1:500	Invitrogen	A22283
Hoechst33342 for fluorescent observation			
Hoechst33342	1:10,000	Invitrogen	H1399
Antibodies for Chromatin immunoprecipitation (ChIP)			
Rabbit anti-pMRLC (Thr18/ser19)	2 μg/1 ChIP	CST	3674
Normal Rabbit IgG #2729	2 μg/1 ChIP	CST	2729

qPCR Primers			
Target Genes	host	Sequences（5' to 3'）	
		Forward	Reverse
CTNNB1 (promoter region)	human	CGGGGTACCTCAGACGGCAGCAGACT	CCCAAGCTTGAGAGGCTTAAAATGGCG
GAPDH	human	TCCTGTTCGACAGTCAGCCGC	TGACCAGGCGCCCAATACGAC
MYL9	human	ACCCACCAGAAGCCAAGATGTC	GGACTGGTCAAACATTGCGAAGAC
MYL12A	human	GCCGGGACTTAACCACCAC	GTTGGATTCTTCCCCAATGAAGC
MYL12B	human	TGCCATGATGAATGAGGCCC	TCCTGAATGGTGCCTGTTGC
ZIPK	human	TCTTCGAGAACAAGAC	CAGCATGATGTTTTCC
MafB	human	ACCAGCTCGTGTCCATGTC	CTGCTGGACGCGTTTATACC
MYO15A	human	ATGCAGCAGATAAAGATCCTGGAG	TGTCGTTCCTGACGGTTTTGG
MYO15B (primer1)	human	CTGGGCCGTATCTATACCTTTGG	GCCACGATGGCAAAGATGTG
MYO15B (primer2)	human	CCTGTCTTGCTTGTTCTGAACCC	ACGATGGCAAAGATGTGTGGAG
MYO18A	human	GCCAGTGAAGCCACATTCAAC	TTCTGCTTTTCCTCAGGCTTGG
MYO18B	human	AGGAACCAGTTCAGCCTCCTTG	GCCATAGAGAAGGCACAGATGC
MYH9	human	TGCTGCACAACCTCAAGGAG	TGGATTGATCTTCTCGGTCTTGC
MYH10	human	AGGCCTGTGAACGAATGATCC	TGCAAACGGCCTGGAAGAAG
MYH14	human	AGTCGTTTGTGGAGAAGGTAGC	TTGGCCTTGTAGTCGACCTTG
s18	mouse	ACTTTTGGGCCTTCGTGTC	GCAAAGGCCCAGAGACTCAT
MafB	mouse	AGGTATAAACGCGTCCAGCAG	TGGCGAGTTTCTCGCACTTG
MYL9	mouse	TTTGGGGAGAAGCTGAACGG	TCCTCGTGGATGAAGCCTGAG
MYL12A	mouse	ACTGCGGAGTCTGGAAAGTTAG	TGGCGGTTAAATCCCTGCTC
MYL12B	mouse	TCTGGGGAAGAATCCCACTGATGC	TAATCCTCCTGGATGGTGCCTGTG

Inhibitors				
Product	Concentration (μM)	reaction time (hour)	Source	Identifier
Blebbistatin (+/-)	25	24	Enzo Life Sciences	BML-EI315
Jasplakinolide	0.1	24	Sigma	J4580
Latrunculin A	10	24	Sigma	L5163
ML-7	10	24	Sigma	I2764
Y-27632	10	24	Sigma	Y0503
ZIPK inhibitor	200	24	Sigma	324788

2-2 Cell culture

Sources of cell lines and primary culture cells are listed below. MSCs were obtained from BALBc mice (BALB/cByJ, female, 7 weeks old, from Jackson laboratory)[17].

Cell line		Source
A431	human epidermoid carcinoma cell line	American Type Culture Collection
A549	human lung adenocarcinoma cell line	American Type Culture Collection
HeLa	human cervical adenocarcinoma cell line	Riken Cell Bank
Primary culture cell		**Source**
HUVECs	Human umbilical vein endothelial cells	Kurabo
MSCs	Mouse mesenchymal stem cells	Gifted by Dr. Suzanne Ponik (University of Wisconsin-Madison)

The media used are listed below. All cells were cultured at 37 °C, 5% CO2.

Cell line	culture medium
A431	Dulbecco's modified Eagle's medium (Sigma-Aldrich, St. Louis, MO, USA) supplemented with 10% fetal bovine serum (172012, Sigma-Aldrich) and 1% antibiotic/antimycotic solution (Sigma-Aldrich)
A549	
HeLa	
Primary culture cell	**culture medium**
HUVECs	ndothelial cell growth medium 2 (C-22111, Promocell Co., Heidelberg, Germany)
MSCs	Dulbecco's modified Eagle's medium (Sigma-Aldrich) supplemented with 20% fetal bovine serum (172012, Sigma-Aldrich) and 1% antibiotic/antimycotic solution (Sigma-Aldrich).

2-3 Cell culture substrates

Plastic or glass dishes coated with 300 μg/mL collagen-I (Nitta Gelatin, Osaka, Japan) were used as stiff substrates. Polyacrylamide gels were prepared using the following reagents (0.4 kPa: 0.05% N,N′-methylenebisacrylamide (BIS) and 5.0% acrylamide; 271 kPa: 0.6% BIS and 12% acrylamide. The procedure for preparing the polyacrylamide gel conformed to a previous study[18]. Atomic force

microscopy was utilized to measure the surface stiffness of the polyacrylamide gels.

	0.4 kPa polyacrylamidogel			271 kPa polyacrylamidogel																				
	Young's modurus（Pa）			Young's modurus（$\times 10^3$ Pa）																				
	observation1	observation2	observation3	observation1							observation2							observation3						
1	671	267	502	1	231	17	274	33	317	49	279	1	330	17	251	33	322	49	263	1	251	17	286	33	268	49	252
2	580	268	529	2	279	18	238	34	285	50	261	2	221	18	216	34	324	50	275	2	289	18	297	34	277	50	284
3	611	263	439	3	258	19	274	35	290	51	248	3	252	19	261	35	283	51	314	3	251	19	260	35	282	51	207
4	574	268	438	4	337	20	294	36	264	52	297	4	271	20	268	36	251	52	262	4	308	20	293	36	298	52	310
5	633	276	382	5	313	21	280	37	243	53	249	5	269	21	281	37	288	53	278	5	256	21	256	37	298	53	258
6	601	285	461	6	276	22	318	38	269	54	231	6	205	22	260	38	284	54	257	6	260	22	246	38	194	54	291
7	616	268		7	300	23	325	39	280	55	271	7	264	23	304	39	278	55	290	7	269	23	338	39	239	55	240
8	639	267		8	296	24	285	40	264	56	260	8	258	24	302	40	303	56	251	8	268	24	282	40	255	56	261
9	642	293		9	251	25	288	41	223	57	286	9	268	25	294	41	292	57	285	9	265	25	275	41	259	57	277
10	595	252		10	291	26	249	42	268	58	275	10	241	26	247	42	309	58	294	10	263	26	277	42	273	58	245
11	676	290		11	279	27	296	43	258	59	262	11	259	27	287	43	261	59	273	11	272	27	331	43	241	59	258
12	628	262		12	264	28	276	44	265	60	259	12	255	28	256	44	267	60	217	12	301	28	294	44	230	60	217
13		261		13	345	29	268	45	233	61	257	13	255	29	296	45	294	61	254	13	218	29	198	45	286	61	267
14				14	299	30	310	46	269	62	266	14	263	30	262	46	334	62	260	14	225	30	204	46	276	62	252
15				15	254	31	271	47	292	63	244	15	289	31	289	47	360	63	267	15	263	31	271	47	253	63	258
16				16	287	32	310	48	253	64	276	16	333	32	273	48	273	64	245	16	306	32	249	48	231	64	251
Average	622	271	458	275							275									264							
Average of 3 observation	450			271																							
Standard deviation	176			6																							

	1.2 kPa polyacrylamidogel			2.3 kPa polyacrylamidogel			25 kPa polyacrylamidogel		
	Young's modurus（Pa）			Young's modurus（Pa）			Young's modurus（Pa）		
	observation1	observation2	observation3	observation1	observation2	observation3	observation1	observation2	observation3
1	1266	1234	1192	2304	2082	2379	25094	25790	25694
2	1255	1197	1262	2371	2113	2367	24265	25694	25780
3	1232	1209	1178	2309	2058	2303	26727	24413	25336
4	1238	1246	1146	2126	2234	2326	24451	22356	26751
5	1252	1189	1287	2316	2000	2338	23537	25836	28074
6	1259	1209	1244	2445	2069	2297	26805	25553	28644
7	1226	1235	1193	2457	2065	2331	23967	24598	26793
8	1230	1316	1173	2249	2135	2492	20526	24812	26656
9	1271	1197	1225	2441	2169	2255	21915	27189	26405
10	1252	1200	1364	2436	2207	2308	24157	26491	27750
11	1232	1213	1192	2349	2291	2527	30813	26764	25865
12	1220	1330	1162	2339	2264	2661	19602	26442	26431
13	1270	1187	1183	2480	2263	2218	20440	26713	
14	1291	1168	1172	2466	2342	2461	24372	25758	
15	1229	1206	1161	2407	2456	2722			
16	1223	1308	1169	2386	2436	2749			
Average	1247	1228	1206	2368	2199	2421	24048	25601	26682
Average of 3 observation	1227			2329			25443		
Standard deviation	20			116			1324		

	61 kPa polyacrylamidogel			83 kPa polyacrylamidogel			134 kPa polyacrylamidogel		
	Young's modurus（Pa）			Young's modurus（Pa）			Young's modurus（Pa）		
	observation1	observation2	observation3	observation1	observation2	observation3	observation1	observation2	observation3
1	63703	65464	64909	81832	73843	92066	131155	132182	140372
2	65595	63892	57912	80386	79391	86330	123964	130869	147846
3	64058	64034	65021	74731	73572	87568	146293	120081	157140
4	59764	64810	65878	77431	80661	97728	137199	119565	160753
5	65333	66265	58240	87489	74037	101888	129129	126708	131741
6	65418	60514	68843	80980	79988	90742	129219	127388	133748
7	65263	59134	64795	77926	77039	92846	156365	116083	159137
8	64025	59205	62578	75694	80669	88877	161540	125827	158791
9	60762	62197	54550	78797	79132	85110	122408	126776	120077
10	64036	55074	62253	83778	80554	94486	142108	113690	141171
11	66027	51914	60611	77360	77020	90142	129076	112099	148232
12	66184	59004	57587	80227	79920	96050	180155	124953	137112
13	55796	62633	52431	80362	73431	98399	127245	111028	117866
14	58050	55639	59007	83463	78854	85601	130763	136657	131320
15	61625	48124	57789	75671	75847	82417	124935	134832	131608
16	62107	61101	63795	81659	79945	87510	138476	123216	134432
Average	62984	59938	61012	79862	77744	91110	138127	123872	140709
Average of 3 observation	61311			82905			134236		
Standard deviation	1545			7184			9068		

2-4 Atomic force microscopy (AFM)

The surface stiffness of the gels was assessed employing atomic force microscopy AFM (Nanowizard4, Bruker, Billerica, MA, USA) using a microscope (TE300, NIKON SOLUTIONS CO., LTD., Tokyo, Japan). Silicon nitride cantilevers of pyramidal shape (MLCT; Bruker) possessing a spring constant of 0.01 N/m, calibrated through thermal tuning via a simple harmonic oscillator model, were utilized. Samples were indented with a calibrated force of 0.2 nN (for 0.4 kPa gel) or 0.5 nN (for 1.2, 2.3, 25, 61, 83, 134, or 271 kPa gels) in a scan area of 1 μm^2 (4 pixels × 4 lines for 0.4, 1.2, 2.3, 25, 61, 83, 134 kPa gels or 8 pixels × 8 lines for 271 kPa gel). Young's modulus were estimated using the Hertzian model, assuming a Poisson's ratio of 0.5. The analysis was conducted using JPK Data Processing software provided by Bruker. The measurement results are shown below.

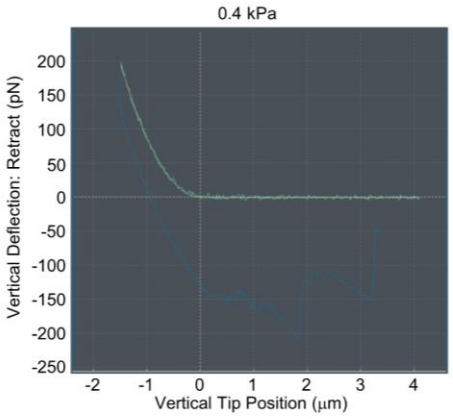
0.4 kPa
Vertical Deflection: Retract (pN)
Vertical Tip Position (μm)

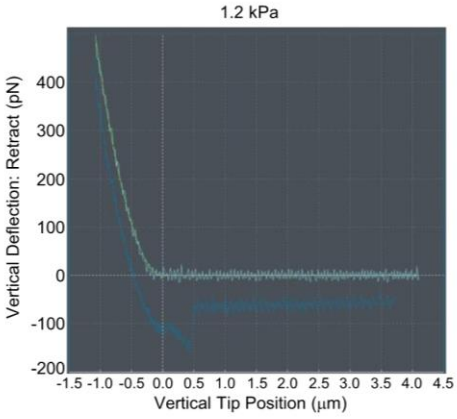
1.2 kPa
Vertical Deflection: Retract (pN)
Vertical Tip Position (μm)

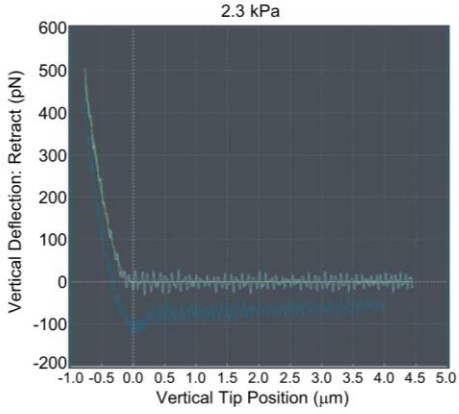
2.3 kPa
Vertical Deflection: Retract (pN)
Vertical Tip Position (μm)

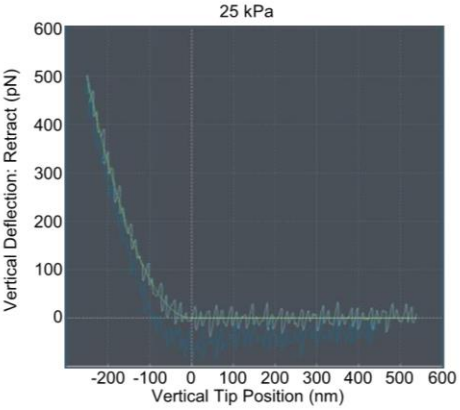
25 kPa
Vertical Deflection: Retract (pN)
Vertical Tip Position (nm)

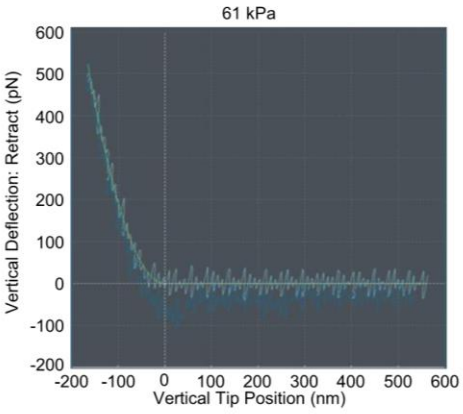
61 kPa
Vertical Deflection: Retract (pN)
Vertical Tip Position (nm)

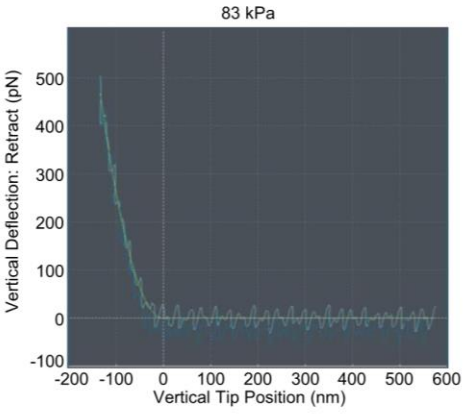
83 kPa
Vertical Deflection: Retract (pN)
Vertical Tip Position (nm)

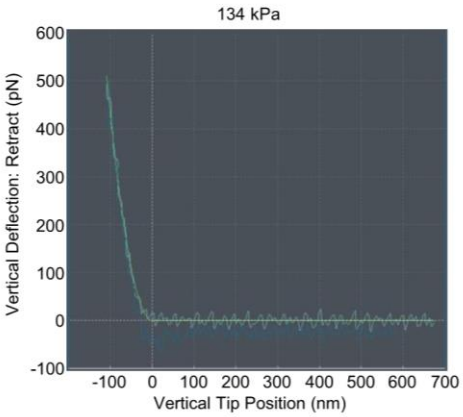
134 kPa
Vertical Deflection: Retract (pN)
Vertical Tip Position (nm)

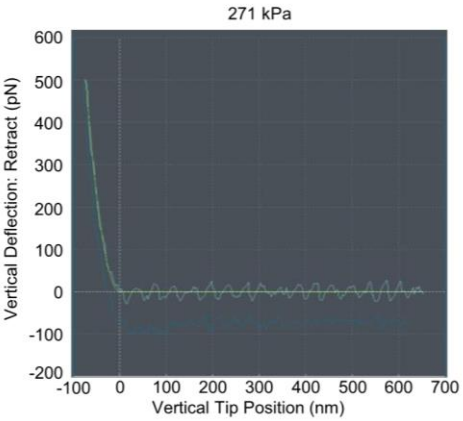
271 kPa
Vertical Deflection: Retract (pN)
Vertical Tip Position (nm)

2-5 Immunofluorescence

Immunofluorescence was performed according to the following procedure.

	Procedure	Temperature	Time	Reagent/Equipment
1	Fixation	Room temp.	10 min	4% paraformaldehyde (Nacalai tesque, INC., Kyoto, Japan) in PBS
2	Wash (3 time)		—	PBS
3	Permeabilization		10 min	1.0 % Triton-X100 in PBS
4	Wash (3 time)		—	PBS
5	Blocking		1 hour	1% bovine serum albumin (FUJIFILM Wako Pure Chemical Corporation)
6	Primary antibody reaction	4° C	Overnight	Listed in "2-1 Reagent"
7	Wash (3 time)	Room temp.	—	PBS
8	Secondary antibody reaction		1 hour	Alexa Fluor-488 anti-mouse IgG or Alexa Fluor-488 anti-rabbit IgG in PBS *Alexa Fluor-546 phalloidin and hoechst33342 added as needed
9	Wash (3 time)		—	PBS
10	Observation		—	A1R confocal imaging system (NIKON SOLUTIONS CO., LTD.)

For the quantification of MRLC's nuclear localization, the MRLC intensity was determined by calculating the ratio between its presence in the nucleus and the cytoplasm. This was achieved using ImageJ software[19].

2-6 Small interfering RNA (siRNA) transfection

Cells were transfected with the appropriate siRNA or non-targeting RNA as a negative control using Lipofectamine RNAiMAX reagent (Thermo Fisher Scientific, Waltham, MA, USA). The siRNAs were generated with in vitro transcription T7 kit (Takara Bio Inc., Shiga, Japan) by using the following sequences.

Target gene name	species	sense sequence (5' to 3')
MYL9	human	TGATAAGAAAGGCAACTTCAACCCTATAG
MYL12A		ACCATGTTTGGTGAGAAGTTACCCTATAG
MYL12B		TTCCAGTTACATTGTCTTACTCCCTATAG
DAPK1		TAGCTGAAAAGGAATCTTTAACCCTATAG
MafB		ACCAATGCATTGCGTTTCTTTCCCTATAG
MYH9		AGCCAACATTGAGACTTATCTCCCTATAG
MYH10		AAGTCTGATTTGCTTCTTGAACCCTATAG
MYO15A		CACCTCTTTGCTGTTGCAAATCCCTATAG
MYO18A		CACATTCAACGTCTTCTACTACCCTATAG
MYL9	mouse	GGCCTTCAACATGATTGATCACCCTATAG
MYL12A		TTCTGTCATTGTGATGAGAAACCCTATAG
MYL12B		CACTTAGCATGTGCATAATCACCCTATAG
non-targeting RNA	—	AAACTACATGTCACATCACGG CCCTATAG

ZIPK siRNA was purchased from Dharmacon (Lafayette, CO, USA). siMRLC was prepared as a mixture of equal amounts of siMYL9, siMYL12A, and siMYL12B.

2-7 Vector transfection

Cells were transfected with GFP-encoding vector (632484, Takara Bio Inc.) or GFP-MafB-encoding vector (MG204681, ORIGENE) with Xfect transfection reagent (Takara Bio Inc.).

2-8 Western blotting

To prepare, cells underwent a single wash with cold PBS, followed by lysis in sodium dodecyl sulfate (SDS) buffer (0.125 M Tris–HCl, 0.2 M dithiothreitol, 4% SDS, 20% glycerol, and 0.01% bromophenol blue, pH 6.8). The cell lysates were then heated at 95°C for 5 minutes. Equivalent

volumes of these lysates were segregated on 8%, 10%, 12%, or 14% SDS-polyacrylamide gels and subsequently transferred onto polyvinylidene fluoride membranes (Merck Millipore, Billerica, MA, USA). Following this, the membrane was obstructed using 1% skim milk in Tris-buffered saline-Tween solution (TBS-T; 10 mM Tris–HCl containing 150 mM NaCl and 0.05% Tween 20, pH 7.5). Blots were treated with primary antibodies, diluted in TBS-T or Can Get Signal Immunoreaction Enhancer Solution 1 (Toyobo, Osaka, Japan), and kept at 4°C overnight. Post-incubation, membranes were washed thrice with TBS-T, and secondary antibodies, employed at the same dilution as primary antibodies, were added. This secondary antibody incubation occurred in TBS-T or Can Get Signal Immunoreaction Enhancer Solution 2 (Toyobo) for 1 hour at room temperature. Protein signals were detected through Immobilon Western Chemiluminescent HRP substrate (Merck Millipore). GAPDH immunocomplexes served as internal standards to ensure equal loading. Concurrently, LaminA/C immunocomplexes were employed as nuclear internal standards to ensure uniform nuclear extraction loading. Furthermore, α-tubulin or GAPDH immunocomplexes were used as cytosolic internal standards to ensure uniform cytosol extraction loading. Blot images were captured using the ChemiDoc Touch Imaging System (Bio-Rad Laboratories Inc., Hercules, CA, USA), and signal intensity was quantified using Image Lab software (Bio-Rad) and normalized to the control value (Relative expression).

2-9 Nuclear/Cytosolic fraction

The isolation of nuclear and cytosolic extracts was carried out utilizing the nuclear/cytosolic fractionation kit (AKR-171, Cell Biolabs, Inc. San Diego, CA, USA). Lamin A/C served as the loading control for nuclear extracts, while α-tubulin and GAPDH were utilized as loading controls for the nuclear and cytosolic extracts, respectively.

2-10 Quantitative PCR (qPCR)

The RNA extraction utilized the FastGene FastGene™ RNA Basic Kit (FG-80250, Nippon Genetics Co., Ltd., Tokyo, Japan). Subsequent reverse transcription was conducted using the ReverTra Ace qPCR RT Kit (FSQ-201, TOYOBO). For qRT-PCR analysis, the KAPA SYBR Fast qPCR kit (Kapa Biosystems, Inc., Woburn, MA, USA) was employed in conjunction with the Applied Biosystems StepOnePlus™ Real-Time PCR System (Thermo Scientific). Primer sequences are following.

qPCR Primers			
Target Genes	host	Sequences（5' to 3'）	
		Forward	Reverse
GAPDH	human	TCCTGTTCGACAGTCAGCCGC	TGACCAGGCGCCCAATACGAC
MYL9	human	ACCCACCAGAAGCCAAGATGTC	GGACTGGTCAAACATTGCGAAGAC
MYL12A	human	GCCGGGACTTAACCACCAC	GTTGGATTCTTCCCCAATGAAGC
MYL12B	human	TGCCATGATGAATGAGGCCC	TCCTGAATGGTGCCTGTTGC
DAPK1	human	GCTGCAAATGATCCCACGTC	ACCGAAGGCTATGGGTTCTTC
ZIPK	human	TCTTCGAGAACAAGAC	CAGCATGATGTTTTCC
MafB	human	ACCAGCTCGTGTCCATGTC	CTGCTGGACGCGTTTATACC
s18	mouse	ACTTTTGGGCCTTCGTGTC	GCAAAGGCCCAGAGACTCAT
MafB	mouse	AGGTATAAACGCGTCCAGCAG	TGGCGAGTTTCTCGCACTTG
MYL9	mouse	TTTGGGGAGAAGCTGAACGG	TCCTCGTGGATGAAGCCTGAG
MYL12A	mouse	ACTGCGGAGTCTGGAAAGTTAG	TGGCGGTTAAATCCCTGCTC
MYL12B	mouse	TCTGGGGAAGAATCCCACTGATGC	TAATCCTCCTGGATGGTGCCTGTG

2-11 Chromatin Immunoprecipitation (ChIP)

The ChIP procedure was performed using the SimpleChIPR Plus Enzymatic Chromatin IP Kit (Magnetic Beads) (9005S, Cell Signaling Technology). For the subsequent PCR analysis, 2 μL of the eluted DNA underwent 40 cycles of amplification using CTNNB1 core promotor-specific primers from previous studies [20] in conjunction with the KAPA SYBR Fast qPCR kit (Kapa Biosystems, Inc.). The resulting PCR products were visualized after running on an agarose gel electrophoresis system and staining with Midori Green Advance (NE-MG04, NIPPON Genetics).

2-12 Death cell rate measurement

Dead cell rate was measured using Trypan Blue (T10282, Thermo Scientific) Cells were reacted with 0.2% Trypan Blue solution for 5 minutes.. A minimum of 500 cells was enumerated using a counting chamber, and the percentage of cells exhibiting Trypan Blue staining was calculated.

2-13 Immunohistochemistry

Formalin-fixed paraffin-embedded tissue sections obtained from tumor samples developed in the KPC autochthonous mouse model of pancreatic ductal adenocarcinoma[21] were deparaffinized, followed by antigen retrieval by boiling the samples in Target-Retrieval Solution (Dako An Agilent

Technologies Company, Carpinteria, CA, USA) at pH 9 for 30 min and conventional staining procedures, as described previously[21], using an anti-phospho-myosin light chain 2 (Thr18/Ser19) (3674S, Cell Signaling Technology) antibody. Mouse spinal cord tissues were fixed in 4% (w/v) PFA overnight, dehydrated in serial methanol washes, and embedded in paraffin. Serial sections (6 μm) embedded in paraffin were prepared for immunohistochemical analysis. Primary antibody against 2P-MRLC (3674S, Cell Signaling Technology) was used with 1% goat serum in PBS. Antigen retrieval was performed using citrate buffer, incubated at 121 °C for 1 min. Primary antibodies were detected using Alexa Fluor 546-conjugated IgG (Molecular Probes, Oregon, USA) and counterstained with Hoechst 33342 (Sigma-Aldrich). The fluorescent signal was visualized using an Olympus BX51 fluorescence microscope, and images were captured using cellSens Standard 1.6 (Olympus Corporation, Tokyo, Japan) software.

2-14 Statical analysis

Each experiment that performed statical analysis was carried out at least three times independently. P-values less than 0.05 were considered statistically significant. Regarding western blotting experiments, statistical significance was determined with a 95% confidence except Fig. 3.13, Fig. 4.7B. In other experiments, statistical significance was performed with Welch's t-tests or Student's t-test. F-test was used to determine if the variances of the data were equal or not.

Chapter 3

Actin fiber formation induced by substrate stiffness promoted the nuclear localization of 2P-MRLC via ZIPK

3-1 Introduction

3-1-1 Myosin regulatory light chain (MRLC)

Myosin regulatory light chain (MRLC), also known as MLC2, RLC, or LC20, plays a critical role in myosin II within cells, primarily found in stress fibers. Phosphorylation at Ser19 (1P-MRLC) or Thr18/Ser19 (2P-MRLC) strengthens the formation of robust stress fibers and enhances myosin II's ATPase activity, increasing contractile force[22,23]. There are three MRLC isoforms (MRLC1, MRLC2, and MRLC3) in human, all of which undergo phosphorylation at Thr18/Ser19[24]. Recent studies have identified 2P-MRLC not only within stress fibers but also inside the cell nucleus[25]. MRLC functions as a transcription factor[20,25,26] (Fig. 3.1). It binds to the core promoter of intercellular adhesion molecule 1 (ICAM-1)[25]. In addition, ICAM-1 promoter activity was governed by phosphorylation/dephosphorylation of MRLC[25]. Ser19-phosphorylated MRLC activates the XO gene by binding to the XO promoter [26]. Despite indications of phosphorylation's role in nuclear MRLC function, specifics regarding its nuclear localization mechanisms remain unclear. Elevated levels of nuclear MRLC di-phosphorylation occur during myocardial ischemia/reperfusion[26,27]. MRLC has only the EF hand domain and phosphorylated region, and does not contain sequences necessary for nuclear transition (Fig. 3. *2*). 2P-MRLC has been reported to be translocated into the nucleus, but the mechanism of this translocation has not been clarified. Notably, it is suggested that

substrate stiffness plays a role in promoting the di-phosphorylation of 2P-MRLC[28], potentially influencing the nuclear localization of MRLC.

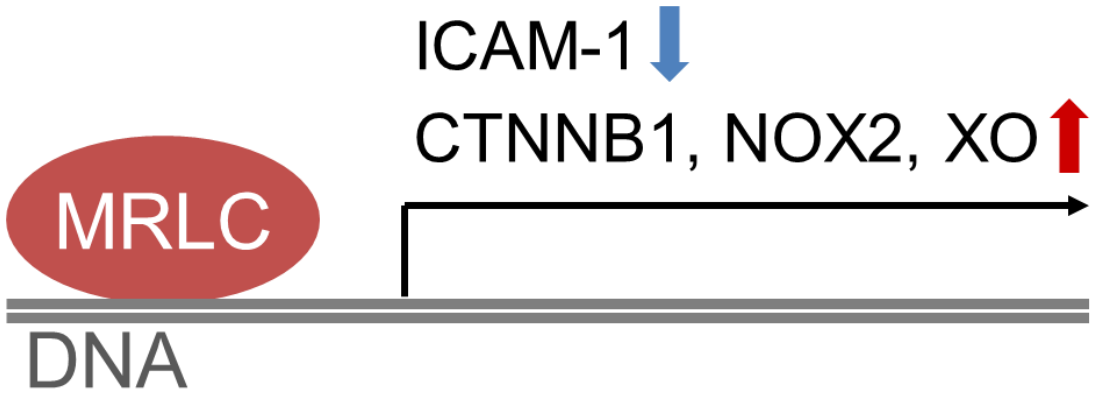

Fig. 3.1 MRLC works as a transcription factor

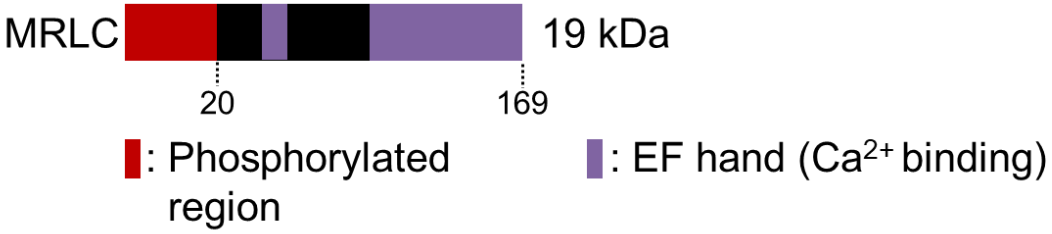

Fig. 3. 2 Domain of MRLC

3-1-2 Zipper-interacting protein kinase (ZIPK)

Zipper interacting protein kinase (ZIPK), also referred to as Death associated protein kinase 3 (DAPK3), is part of the DAPK protein family and is primarily involved in regulating cellular death processes[29]. Recent research has shed light on an additional function of ZIPK, specifically in promoting the di-phosphorylation of MRLC[30]. ZIPK contains a nuclear localization signal (NLS) sequence crucial for its translocation into the nucleus[31]. Studies have demonstrated that the

dephosphorylation of T299 or the inactivation of the leucine zipper (LZ) domain in ZIPK facilitates its entry into the nucleus[32,33]. It has been suggested that the dephosphorylation of Thr299 augments the nuclear localization of ZIPK through the second NLS among its four NLSs[32,33]. Thus, ZIPK has the ability to translocate itself into the nucleus and phosphorylate MRLC (Fig. 3. *3*), but it is not clear whether it regulates nuclear MRLC.

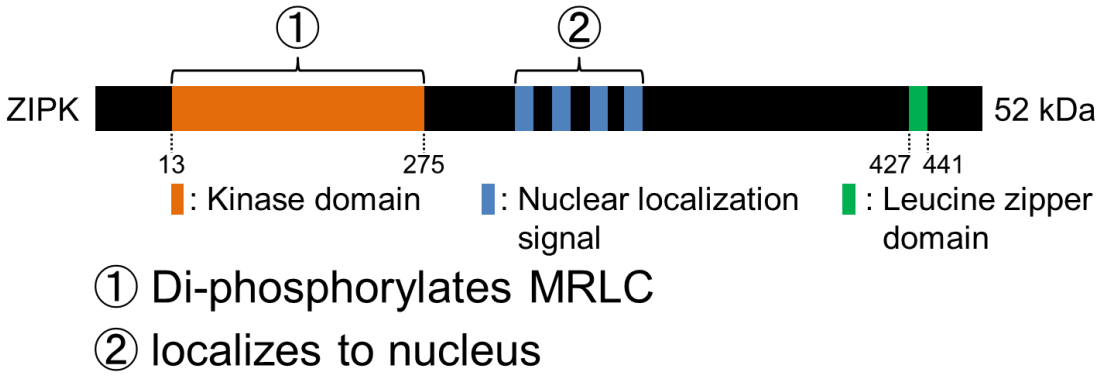

Fig. 3. 3 ZIPK function

3-2 Results

3-2-1 Stiff substrates promote the nuclear localization of 2P-MRLC

Previous studies have indicated the presence of 2P-MRLC inside the nucleus [20], where MRLC functions as a transcriptional regulator and experiences phosphorylation in response to stiff substrates[28]. However, the impact of substrate stiffness on MRLC's nuclear positioning has yet to be explored. Therefore, our investigation focused on tracing the whereabouts of 2P-MRLC in HeLa cells positioned on either stiff or flexible surfaces. Collagen-I-coated polyacrylamide hydrogels were

utilized for these substrates, with the flexible substrate measuring 0.4 kPa and the stiff one measuring 271 kPa. Our observations revealed a notable tendency for 2P-MRLC to accumulate within the nuclei of cells on stiff substrates (Fig. 3.4A and D). While total-MRLC similarly localized to the nuclei on stiff substrates, the rate of this change was relatively lower compared to that of 2P-MRLC (Fig. 3.4C and D). Conversely, the nuclear localization of 1P-MRLC remained unaffected by the stiffness of the substrates (Fig. 3.4B–D). Moreover, immunoblotting using nuclear and cytosolic extracts indicated increased levels of both nuclear and cytosolic 2P-MRLC on stiff substrates (Fig. 3.5A and B). Notably, the expression of 2P-MRLC significantly heightened within the nucleus compared to the cytoplasm in response to the stiff substrates. These findings suggest that the nuclear positioning of MRLC in response to substrate stiffness is regulated by the dually phosphorylated state of MRLC at Thr18 and Ser19. Additionally, our investigations revealed a prominent nuclear localization of 2P-MRLC on stiff substrates in various cell types, including A431 human epidermoid cancer cells, A549 human lung cancer cells, human umbilical vein endothelial cells (HUVECs), and mouse mesenchymal stem cells (MSCs) (Fig. 3.6A-E). These findings propose that substrate stiffness amplifies the nuclear concentration of 2P-MRLC. Finally, our study confirmed distinct alterations in the nuclear positioning of 2P-MRLC across substrates ranging in elasticity from 0.4 kPa to 271 kPa. The outcomes revealed a notable promotion in the nuclear localization of 2P-MRLC as the substrate's stiffness increased from 1.2 to 61 kPa (Fig. 3.7A and B). In contrast, the nuclear concentration of 2P-MRLC exhibited no

significant changes within the range of 61 to 134 kPa (Fig. 3.7A and B). These findings suggest that cells respond to variations in substrate stiffness within the range of 1.2 to 61 kPa, leading to alterations in the nuclear localization of 2P-MRLC.

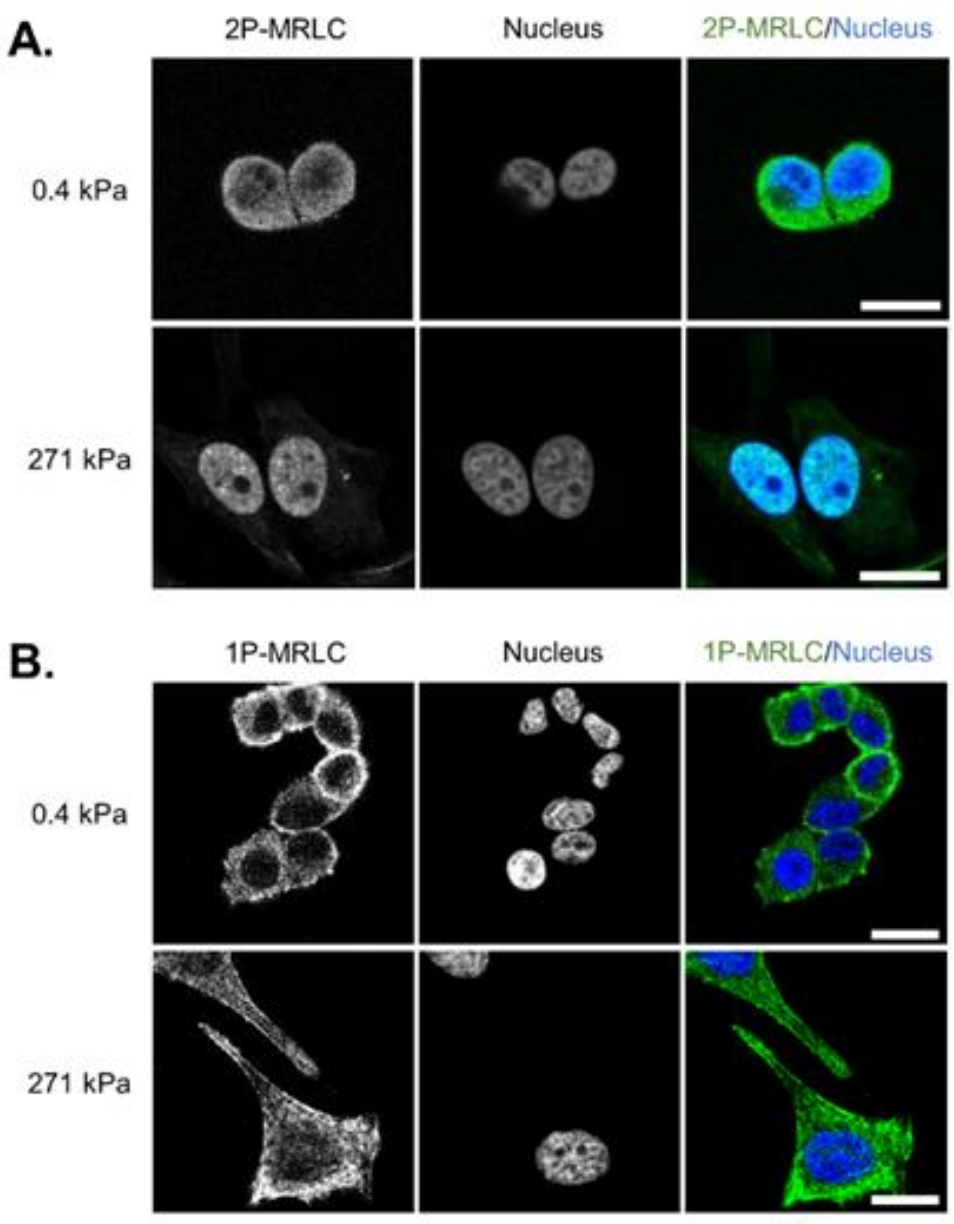

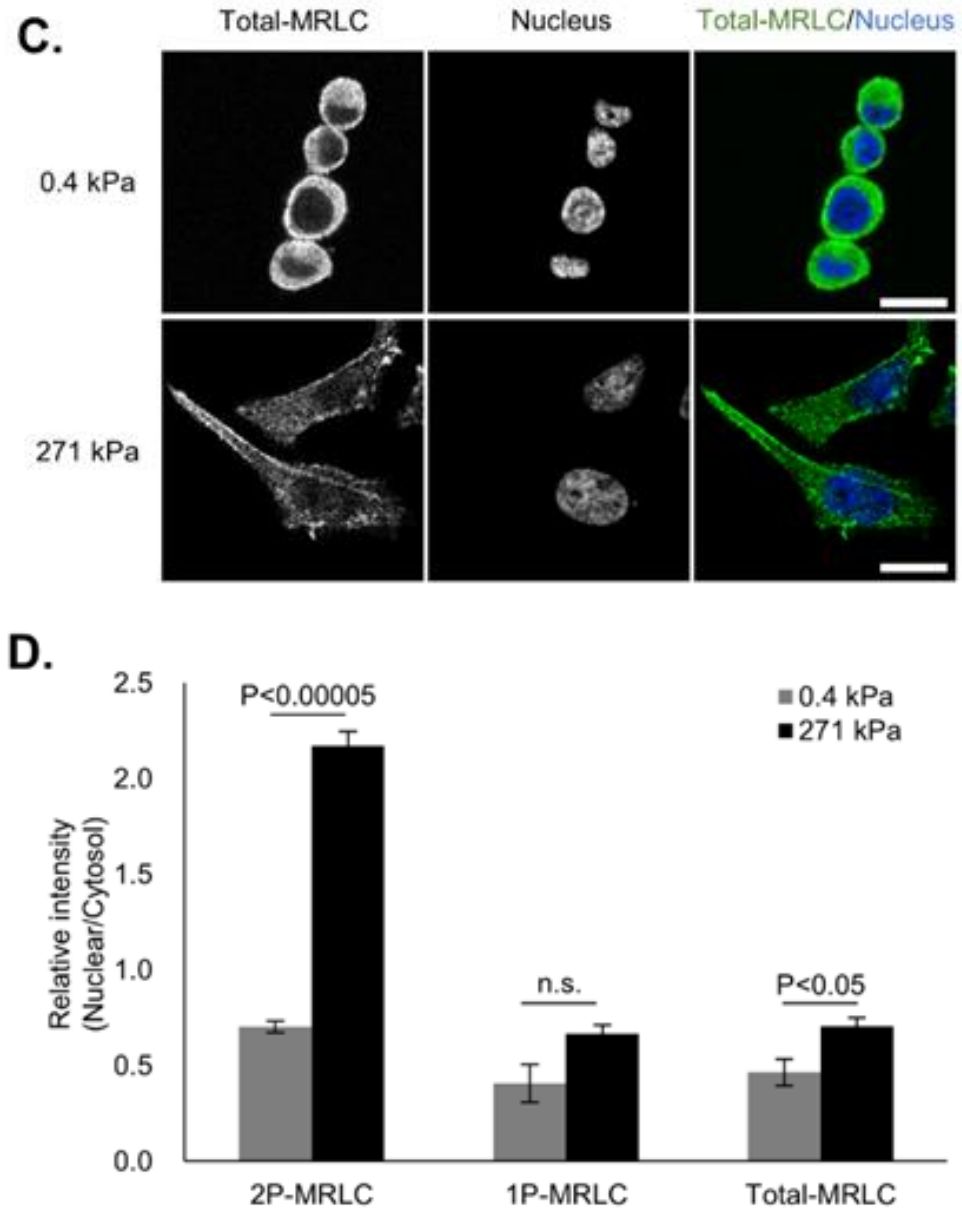

Fig. 3.4 Immunofluorescent staining of 2P-MRLC, 1P-MRLC and Total-MRLC to access the nuclear localization change on soft (0.4 kPa) or stiff (271 kPa) substrates.

(A–C) Illustrative immunofluorescence images of 2P-MRLC (A), 1P-MRLC (B), or total-MRLC (C) alongside the nucleus within HeLa cells, observed on both soft (0.4 kPa) and stiff (271 kPa) polyacrylamide hydrogel substrates coated with collagen I. (D) Quantification of the fluorescent

intensities of 2P-MRLC, 1P-MRLC, and total-MRLC in the nucleus relative to those in the cytosol (A–C). The study encompassed a minimum of 60 cells across three independent experiments. Error bars represent mean ± standard error of the mean (SEM).

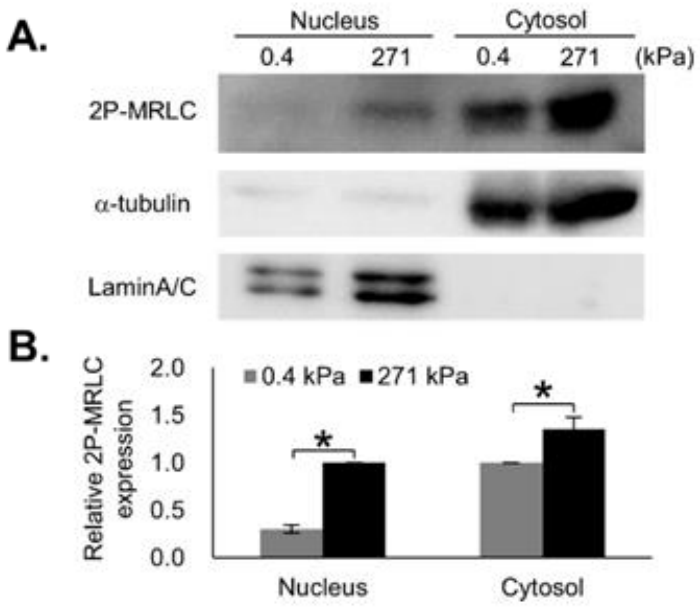

Fig. 3.5 Western blotting for 2P-MRLC to access the nuclear localization change on soft (0.4 kPa) or stiff (271 kPa) substrates.

(A) Exemplary western blots displaying nuclear or cytosolic extracts from HeLa cells cultured on compliant (0.4 kPa) or stiff (271 kPa) polyacrylamide hydrogel substrates coated with collagen-I. The blots were probed with anti-2P-MRLC, anti-α-tubulin, and anti-LaminA/C antibodies. (B) Assessment of relative 2P-MRLC expression from (A). The ratio of 2P-MRLC to the internal control is presented. LaminA/C and α-tubulin were utilized as internal controls for nuclear and cytosolic extracts, respectively. This analysis was conducted in three independent experiments. Error bars indicate the mean ± SEM.

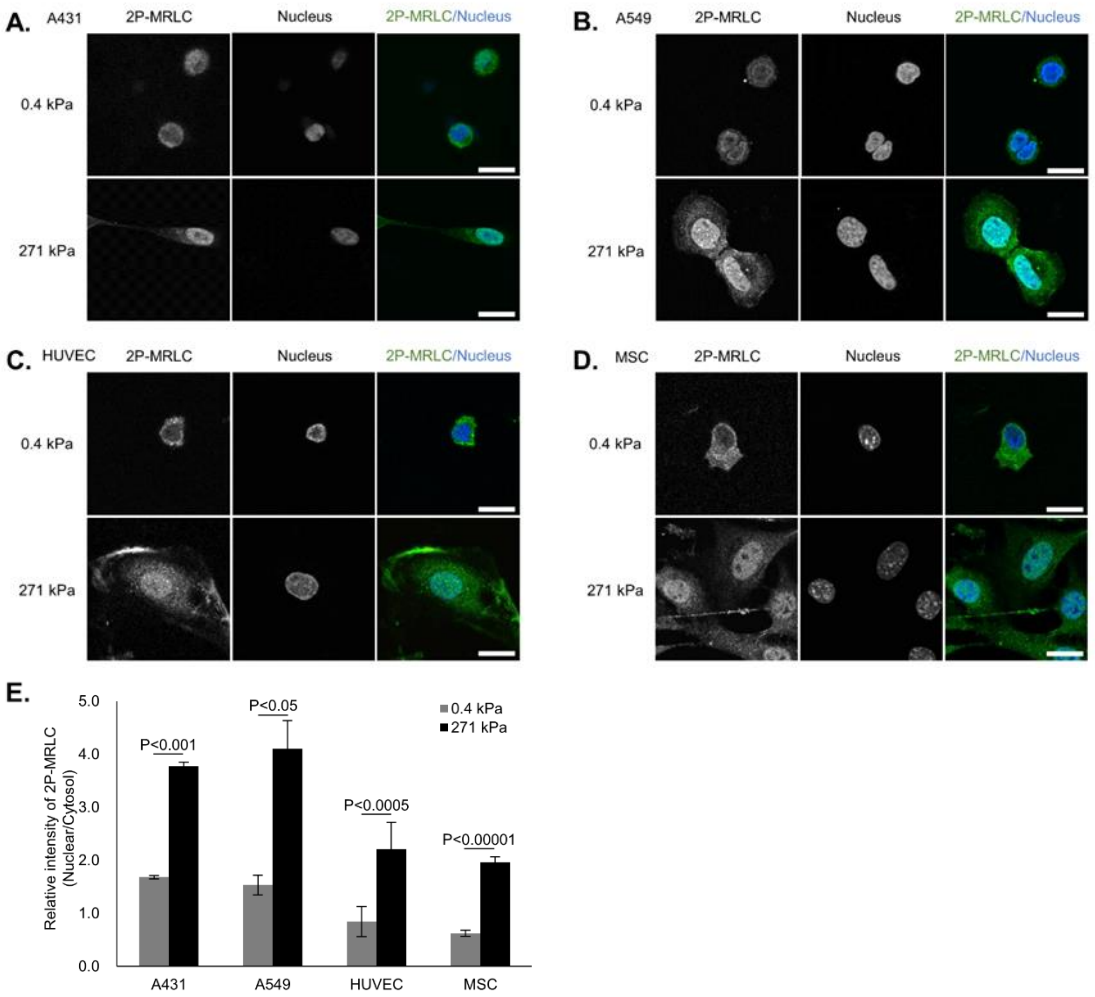

Fig. 3.6 Immunofluorescent staining of 2P-MRLC to access the nuclear localization change on soft (0.4 kPa) or stiff (271 kPa) substrates in various cells or cell lines.

(A–D) Depiction of characteristic immunofluorescence micrographs featuring 2P-MRLC alongside the nucleus within distinct cell types—A431 cells (A), A549 cells (B), human umbilical vein endothelial cells (HUVECs) (C), and mesenchymal stem cells (MSCs) (D)—cultured on compliant (0.4 kPa) or stiff (271 kPa) polyacrylamide hydrogel substrates. The scale bars denote 20 μm. (E) Analysis of the fluorescent intensity quantification of 2P-MRLC in the nucleus relative to the cytosol

across various cell lines and primary cells from A to D. The study encompassed a minimum of 60 cells in three independent experiments. Error bars denote the mean ± SEM.

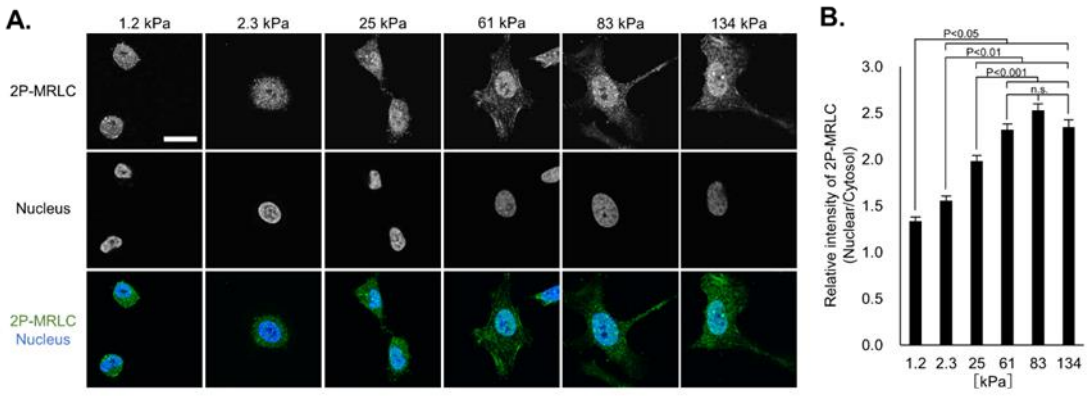

Fig. 3.7 Immunofluorescent staining of 2P-MRLC to access the nuclear localization change in the stiffness range of 1.2 to 134 kPa.

(A) Illustrative immunofluorescent images depicting 2P-MRLC and the nucleus within HeLa cells cultured on polyacrylamide hydrogel substrates of 1.2, 2.3, 25, 61, 83, or 134 kPa, all coated with collagen I. (B) Assessment of the fluorescence intensities of 2P-MRLC in the nucleus relative to those in the cytosol (A). Error bars denote the mean ± SEM.

3-2-2 Nuclear localization of ZIPK regulated by substrate stiffness increases the localization of 2P-MRLC to the nucleus

We directed our attention to ZIPK (DAPK3) in order to unravel how stiff substrates facilitate the nuclear accumulation of 2P-MRLC. ZIPK plays a role in promoting the di-phosphorylation of MRLC[34]. To examine if ZIPK governs the nuclear localization of 2P-MRLC, we utilized specific siRNAs to downregulate ZIPK expression (Fig. 3.8A and B). We assessed the nuclear presence of 2P-MRLC in cells with ZIPK knockdown (KD) and negative control (NC) on stiff glass substrates. Cells with ZIPK-KD displayed a reduction in the nuclear localization of 2P-MRLC (Fig. 3.9A and B). Additionally, we investigated if inhibiting ZIPK activity affected the nuclear localization of 2P-MRLC. Treatment with a ZIPK inhibitor resulted in diminished nuclear localization of 2P-MRLC (Fig. 3.10A and B). Notably, ZIPK inhibitors also impede the activity of death-associated protein kinase 1 (DAPK1)[35]. We further probed the impact of DAPK1 on the nuclear localization of 2P-MRLC by reducing DAPK1 expression using specific siRNAs (Fig. 3.11A). Alterations in the nuclear localization of 2P-MRLC were not observed in DAPK1-KD cells (Fig. 3.11B and C). These outcomes highlight ZIPK's pivotal role in augmenting the nuclear localization of 2P-MRLC, contrasting with the limited effect of DAPK1 on this process. The findings distinctly point to ZIPK as the driver of enhanced nuclear localization of 2P-MRLC.

Our subsequent investigation focused on exploring how substrate stiffness regulates ZIPK activity. ZIPK possesses a nuclear localization signal (NLS) in its amino acid sequence[31]. Given ZIPK's role in di-phosphorylating nuclear MRLC (Fig. 3.10A), we posited that stiff substrates might intensify ZIPK's nuclear presence. To examine this, we examined ZIPK localization in HeLa cells cultivated on either soft (0.4 kPa) or stiff (271 kPa) substrates. Simultaneously, we conducted immunofluorescent staining to assess 2P-MRLC localization in HeLa cells on different substrate stiffities. Our observations unveiled a tendency for ZIPK to preferentially accumulate in the nuclei of cells cultured on stiffer substrates (Fig. 3.12). Furthermore, we performed western blot analyses on nuclear and cytosolic extracts obtained from HeLa cells grown on soft (0.4 kPa) or stiff (1 MPa<) substrates, comparing ZIPK levels in these extracts. Strikingly, ZIPK levels exhibited a significant increase within the nucleus while concurrently decreasing in the cytosol of cells on stiff substrates (Fig. 3.13A and B). distinct molecular weights of ZIPK were observed in the nuclear and cytosolic extracts, as depicted in Fig. 2E. To corroborate this, we observed decreased band intensities for both molecular weights upon ZIPK knockdown using siRNA (Fig. 3.8B). Moreover, treatment with a ZIPK inhibitor led to reduced nuclear ZIPK levels and an increase in cytosolic ZIPK (Fig. 3.14A and B). This differential distribution of ZIPK in the nucleus and cytosol might reflect its active and inactive forms, respectively. These findings underscore the significance of substrate stiffness in regulating the nuclear localization of ZIPK, thereby impacting the nuclear localization of 2P-MRLC.

Our exploration delved into evaluating the impact of other conventional kinases responsible for MRLC regulation, such as myosin light-chain kinase (MLCK) and Rho-associated protein kinase (ROCK), on the nuclear localization of 2P-MRLC[36-38]. Specifically, we examined whether there were alterations in the nuclear localization of 2P-MRLC upon treatment with ML-7 (an MLCK inhibitor) or Y-27632 (a ROCK inhibitor). Surprisingly, neither of these inhibitors affected the nuclear localization of 2P-MRLC (Fig. 3.15A and B). These findings strongly suggest the specificity of ZIPK as the primary kinase responsible for nuclear MRLC dynamics.

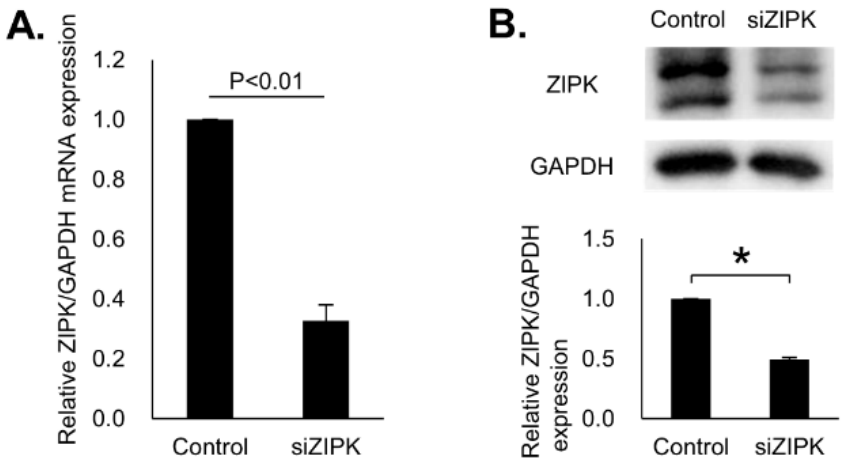

Fig. 3.8 Confirming knockdown efficiency of ZIPK.

(A) Assessment of the relative mRNA expression levels of ZIPK via qPCR in HeLa cells cultivated on stiff plastic substrates subsequent to transfection with either negative control siRNA (control) or siRNA specifically targeting ZIPK (siZIPK). (B) Western blot analysis (above) and quantification (below) of ZIPK protein levels in HeLa cells cultured on plastic substrates post-transfection with

negative control siRNA (control) or siRNA directed against ZIPK (siZIPK). This study was conducted across three independent experiments. Error bars indicate the mean ± SEM. *Statistical significance was assessed at a 95% confidence interval.

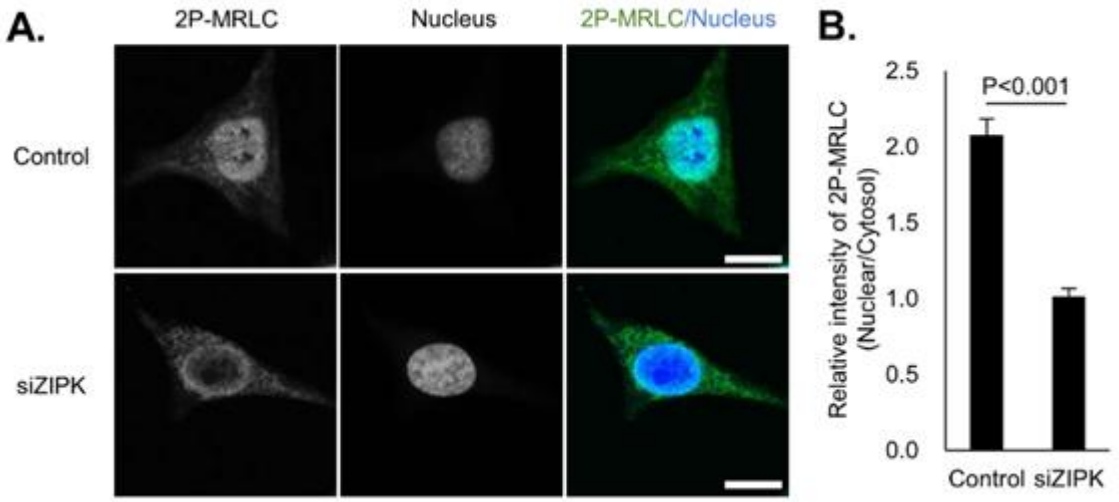

Fig. 3.9 Nuclear localization change of 2P-MRLC dependent on knockdown of ZIPK.

(A) Illustrative immunofluorescent micrographs displaying 2P-MRLC and the nucleus within HeLa cells cultured on stiff glass substrates coated with collagen-I subsequent to transfection with negative control short interfering RNA (siRNA) (control) or siRNA specifically targeting ZIPK (siZIPK). (B) Analysis quantifying the fluorescent intensity of 2P-MRLC in the nucleus relative to that in the cytosol as shown in (A). The study involved a minimum of 60 cells conducted across three independent experiments. Error bars indicate the mean ± SEM.

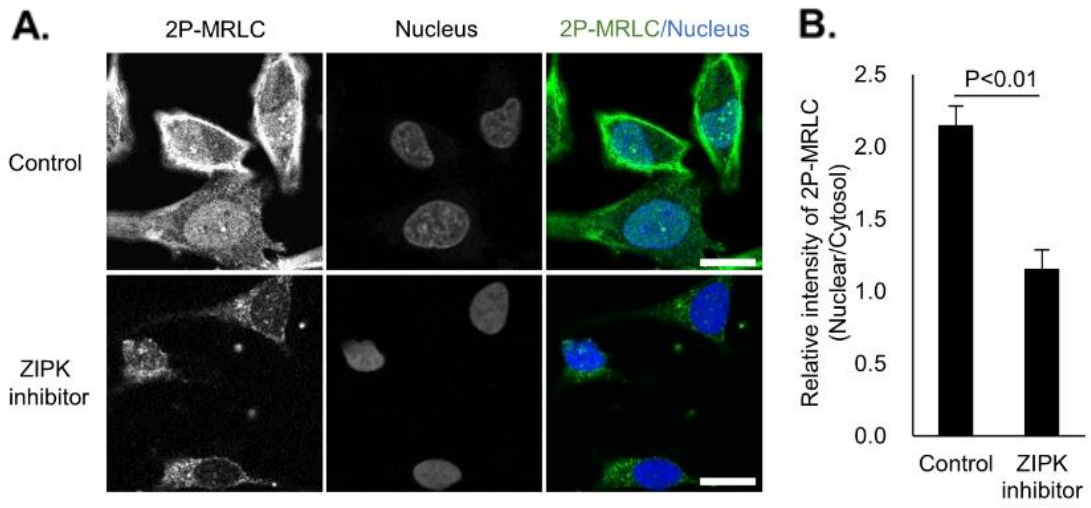

Fig. 3.10 Nuclear localization change of 2P-MRLC dependent on inhibition of ZIPK.

(A) Exemplary immunofluorescent micrographs displaying 2P-MRLC and the nucleus within HeLa cells cultured on stiff glass substrates coated with collagen-I subsequent to treatment with dimethyl sulfoxide (DMSO) (control) or a ZIPK inhibitor. (B) Analysis quantifying the fluorescent intensity of ZIPK in the nucleus relative to that in the cytosol as shown in (A). The study encompassed a minimum of 60 cells conducted across three independent experiments. Error bars indicate the mean ± SEM.

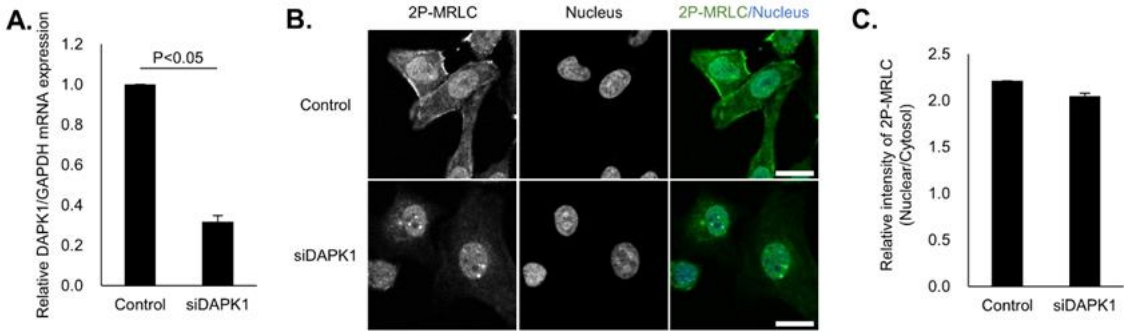

Fig. 3.11 Nuclear localization change of 2P-MRLC dependent on DAPK1 knockdown.

(A) Assessment of the relative mRNA expression levels of DAPK1 via qPCR in HeLa cells cultured on stiff glass substrates coated with collagen-I following transfection with negative control siRNA (control) or siRNA specifically targeting DAPK1 (siDAPK1). The analysis was conducted across three experiments, with statistical significance determined using an unpaired t-test. Error bars represent the mean ± SEM. (B) Depiction of representative immunofluorescent micrographs illustrating 2P-MRLC and the nucleus within HeLa cells on stiff glass substrates coated with collagen-I post-transfection with negative control siRNA (control) or siRNA targeting DAPK1 (siDAPK1). (C) Analysis quantifying the fluorescent intensity of 2P-MRLC in the nucleus relative to the cytosol as depicted in (B). This analysis encompassed at least 40 cells conducted in two independent experiments. Scale bars denote 20 μm. Error bars indicate the mean ± SEM.

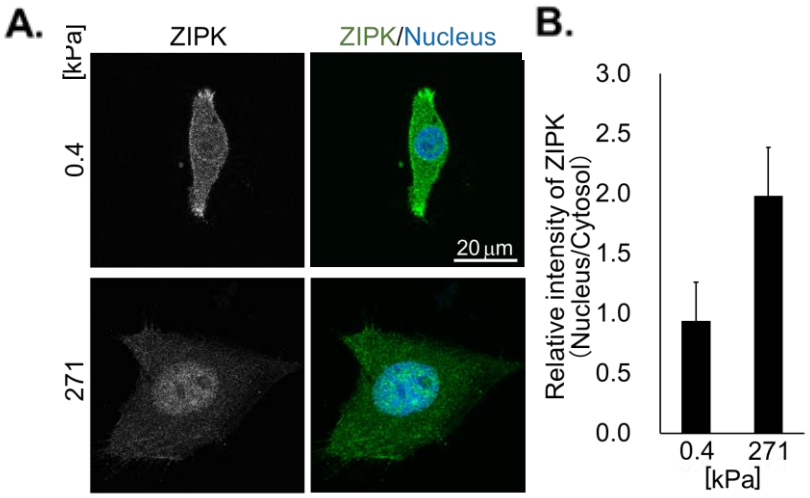

Fig. 3.12 Immunofluorescent staining of ZIPK to access the nuclear localization change on soft (0.4 kPa) or stiff (271 kPa) substrates.

(A) Illustrative western blots displaying nuclear or cytosolic extracts of HeLa cells cultured on compliant (0.4 kPa) or stiff (271 kPa) polyacrylamide hydrogel substrates coated with collagen-I. The blots were probed using anti-2P-MRLC, anti-α-tubulin, and anti-LaminA/C antibodies. (B) Analysis presenting the relative expression levels of 2P-MRLC as observed in (A). The ratio of 2P-MRLC to the internal control is depicted, with LaminA/C and α-tubulin serving as the internal controls for nuclear and cytosolic extracts, respectively. n = 1 experiments.

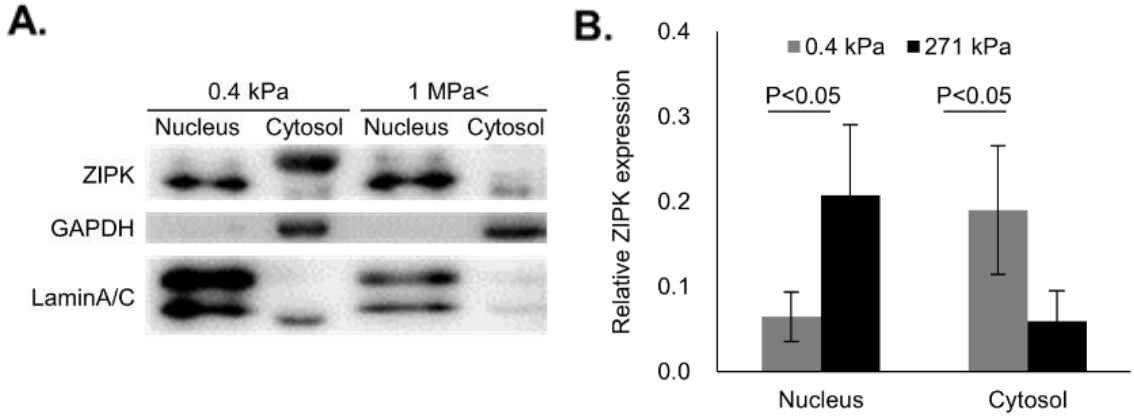

Fig. 3.13 Western blotting for 2P-MRLC to access the nuclear localization change on soft (0.4 kPa) or stiff (1 MPa) substrates.

(E) Representative western blots depicting nuclear or cytosolic extracts of HeLa cells on compliant (0.4 kPa) polyacrylamide hydrogel or stiff plastic (>1MPa) substrates coated with collagen-I using anti-ZIPK, anti-GAPDH, and anti-LaminA/C antibodies. (F) Analysis presenting the relative expression levels of ZIPK as observed in (E). The ratio of ZIPK to the internal control is illustrated, with LaminA/C and GAPDH serving as the internal controls for nuclear and cytosolic extracts, respectively. This analysis encompasses at least three independent experiments.

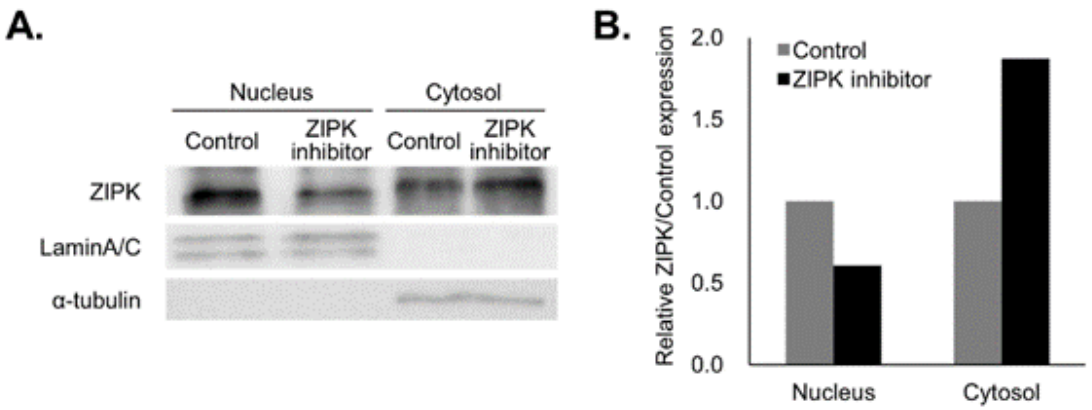

Fig. 3.14 Nuclear localization change of ZIPK depended on its inhibition.

(A) Exemplary western blots displaying the nuclear and cytosolic extracts of HeLa cells cultured on stiff plastic (>1MPa) substrates coated with collagen-I after treatment with DMSO (control) or a ZIPK inhibitor. The blots were probed using anti-ZIPK, anti-α-tubulin, and anti-LaminA/C antibodies. (B) Analysis illustrating the relative expression levels of ZIPK as observed in (A). The ratio of ZIPK to the internal control is depicted, with LaminA/C and α-tubulin serving as the internal controls for nuclear and cytosolic extracts, respectively. This analysis represents a single experiment.

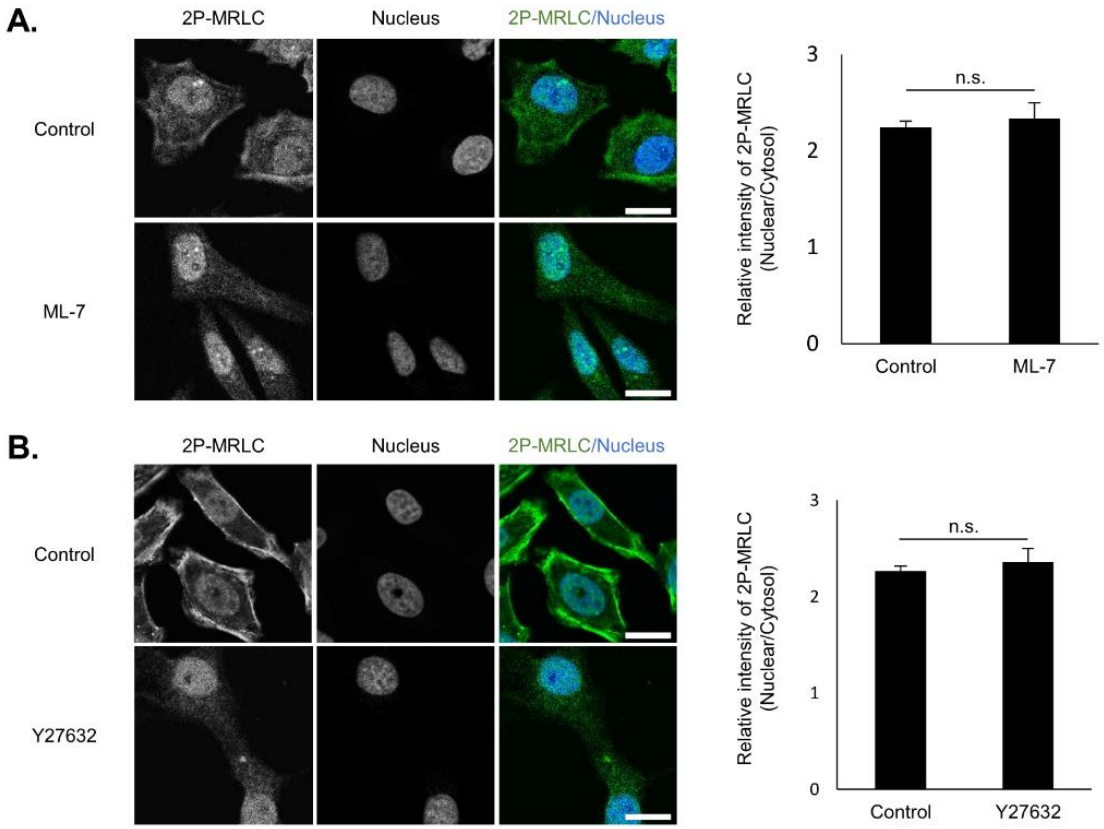

Fig. 3.15 Nuclear localization change of 2P-MRLC depended on inhibition of Myosin light-chain kinase (MLCK), Rho-associated protein kinase (ROCK)

(A–B) Depiction of representative immunofluorescent micrographs displaying 2P-MRLC and the nucleus (left), alongside quantification indicating the fluorescent intensity of 2P-MRLC in the nucleus relative to that in the cytosol (right), observed in HeLa cells on stiff glass substrates coated with collagen-I post-treatment with or without ML-7 (A) and Y27632 (B). Scale bars denote 20 μm. The analysis encompassed a minimum of 60 cells conducted across three independent experiments. Error bars represent the mean ± SEM. Statistical significance was assessed using an unpaired t-test, denoted as n.s. for not significant.

3-2-3 Actin fiber regulates the nuclear localization of 2P-MRLC and ZIPK

Our focus turned to unraveling the intricate mechanisms governing the stiffness-triggered nuclear localization of 2P-MRLC through ZIPK. The actin cytoskeleton, an integral element in sensing and transmitting mechanical cues, plays a pivotal role in mechanotransduction[39]. Previous studies have highlighted the actin cytoskeleton's role in localizing the transcription factor YAP to the nucleus through mechanical stimulation[40]. Conversely, inhibiting actin polymerization has been reported to suppress YAP's nuclear localization in response to stiffness[15]. Based on these findings, we hypothesized that actin filament stabilization, driven by substrate stiffness, governs the nuclear localization of 2P-MRLC and ZIPK.

Initially, we explored the impact of jasplakinolide, an actin depolymerization inhibitor, on the nuclear localization of 2P-MRLC. Interestingly, cells treated with jasplakinolide displayed augmented nuclear localization of 2P-MRLC on softer substrates (Fig. 3.16A and B). Subsequently, we assessed whether treatment with latrunculin A, an actin polymerization inhibitor, modulated the nuclear localization of 2P-MRLC. Cells exposed to latrunculin A exhibited diminished nuclear localization of 2P-MRLC (Fig. 3.17A and B). To consolidate the premise that actin fiber stability fosters the nuclear localization of ZIPK, we conducted western blot analysis of ZIPK levels in nuclear and cytosolic extracts from HeLa cells on stiff substrates treated with or without latrunculin A. Intriguingly, the results demonstrated

decreased ZIPK levels in the nucleus and an increase in the cytosol following latrunculin A treatment (Fig. 3.18A and B). These findings underscore the role of actin fibers in promoting the nuclear localization of ZIPK and 2P-MRLC.

Actin fiber integrity plays a crucial role in sustaining actomyosin contraction, and its stabilization significantly impacts cellular function. Previous studies have highlighted that actomyosin contraction induced by substrate stiffness prompts the activation of transcription factors vital in the mechanotransduction signaling pathway[15,28]. To delve into the influence of contractile forces on the nuclear localization of 2P-MRLC, we explored whether altering contractility using blebbistatin, a myosin II inhibitor, or Y-27632, a ROCK inhibitor, would impact 2P-MRLC localization; both agents are known to inhibit actomyosin contraction[41,42]. Surprisingly, neither blebbistatin nor Y-27632 altered the nuclear localization of 2P-MRLC (Fig. 3.15A and B, Fig. 3.19A and B). These findings suggest that while substrate stiffness-induced actin fiber stabilization fosters the nuclear localization of 2P-MRLC, actomyosin contraction appears to have minimal influence on this localization.

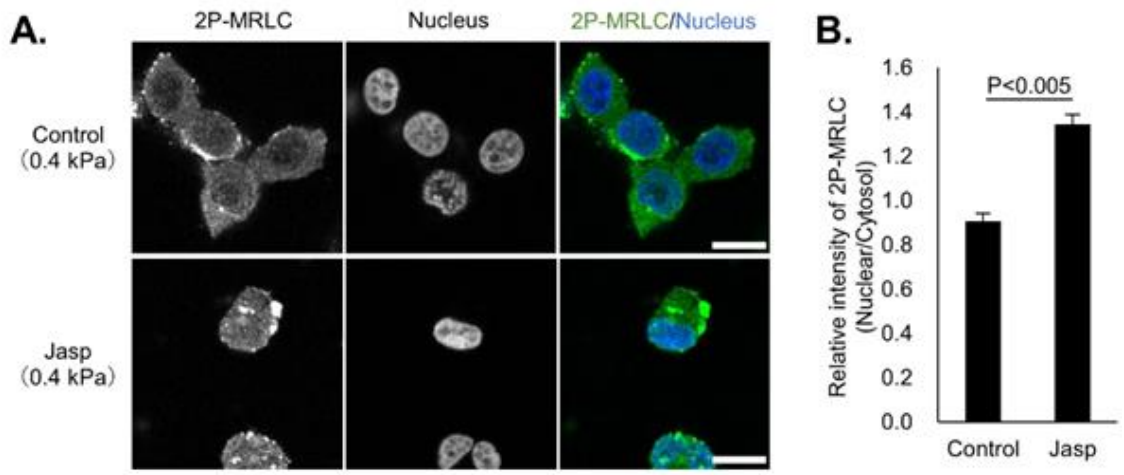

Fig. 3.16 Nuclear localization change of 2P-MRLC depended on actin fiber formation

(A) Depiction of representative immunofluorescent micrographs displaying 2P-MRLC and the nucleus in HeLa cells on compliant (0.4 kPa) polyacrylamide hydrogel substrates coated with collagen-I after treatment with DMSO or jasplakinolide (Jasp). (B) Quantification indicating the fluorescent intensity of 2P-MRLC in the nucleus relative to that in the cytosol as observed in (A). The study involved a minimum of 60 cells conducted across three independent experiments. Scale bars indicate 20 μm. Error bars represent the mean ± SEM. Statistical significance was determined using an unpaired t-test.

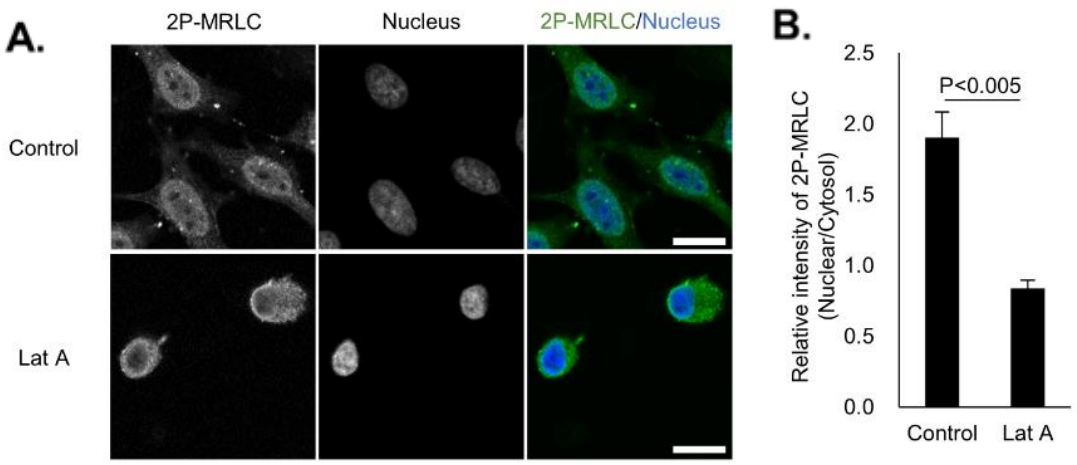

Fig. 3.17 Nuclear localization change of 2P-MRLC depended on inhibition of actin fiber formation.

(A) Illustrative immunofluorescent micrographs exhibiting 2P-MRLC and the nucleus in HeLa cells on stiff glass substrates coated with collagen-I post-treatment with DMSO or latrunculin A (LatA). (B) Analysis quantifying the fluorescent intensity of 2P-MRLC in the nucleus relative to that in the cytosol as depicted in (A). The study involved a minimum of 105 cells conducted across three independent experiments. Scale bars denote 20 μm. Error bars represent the mean ± SEM. Statistical significance was determined using an unpaired t-test.

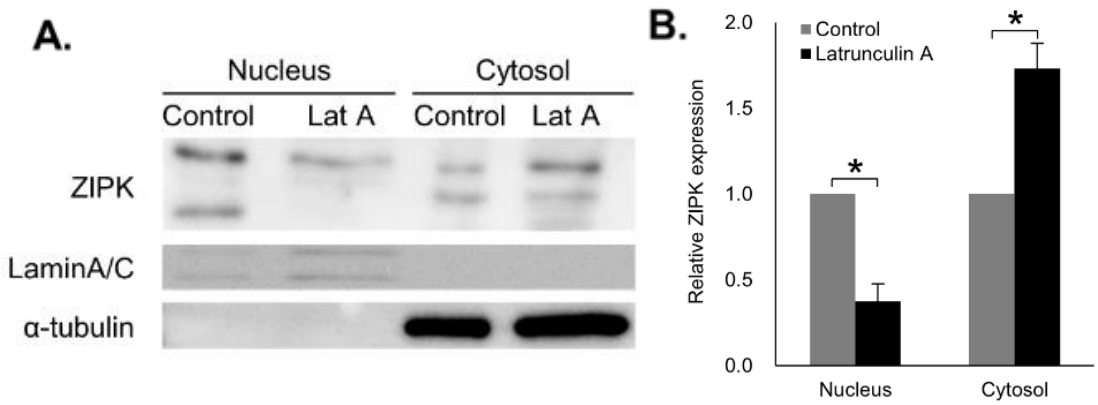

Fig. 3.18 Nuclear localization change of 2P-MRLC depended on inhibition of actin fiber formation.

(A) Exemplary western blots depicting ZIPK in the nuclear or cytosolic extracts obtained from HeLa cells on stiff plastic substrates (>1MPa) coated with collagen-I following treatment with either DMSO (Control) or Latrunculin A (LatA). (B) Analysis illustrating the relative expression levels of ZIPK as observed in (A). The ratio of ZIPK to the internal control is depicted, where LaminA/C and α-tubulin served as the internal controls for nuclear and cytosolic extracts, respectively. This study involved three experiments.

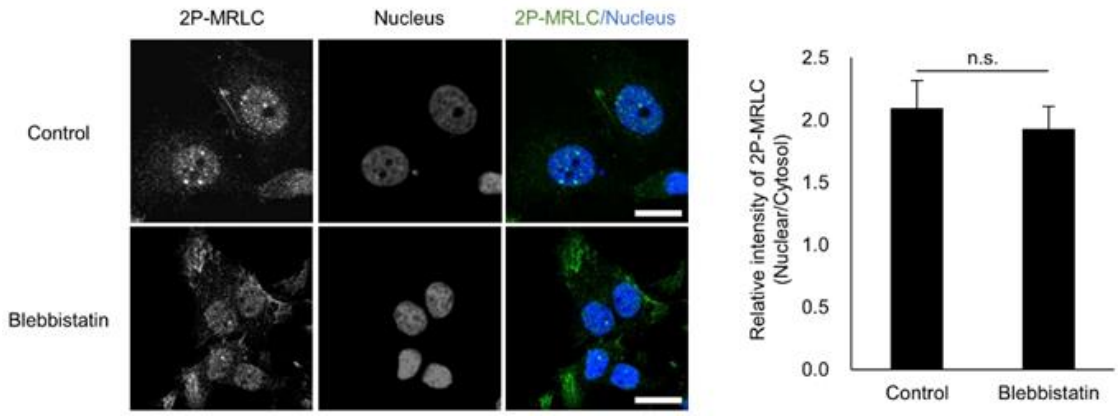

***Fig. 3.19 Nuclear localization change of 2P-MRLC depended on inhibition of myosin-II* activity.**

(Left) Depiction of representative immunofluorescent micrographs illustrating 2P-MRLC and the nucleus, along with (right) quantification indicating the fluorescent intensity of 2P-MRLC in the nucleus relative to that in the cytosol observed in HeLa cells on stiff glass substrates coated with collagen-I following treatment with or without blebbistatin. Scale bars represent 20 μm. The study involved a minimum of 60 cells conducted across three independent experiments. Error bars indicate the mean ± SEM. Statistical significance was assessed using an unpaired t-test, denoted as n.s. for not significant.

3-2-4 Class-2 myosin regulates nuclear localization of 2P-MRLC

We found that substrate stiffness significantly increased the nuclear presence of 2P-MRLC. Previous studies have underscored the role of myosin regulatory light chain (MRLC) as part of the myosin heavy chain subunits[43]. With this knowledge, we delved into whether the nuclear translocation of 2P-MRLC in response to substrate stiffness involves interactions with the myosin family. Myosins known to interact with MRLC and express within the nucleus include classes -2 (MYH9, MYH10, MYH14), -15 (MYO15A, MYO15B), and -18 (MYO18A, MYO18B)[20,43,44]. To begin, we validated the expression of MYH9, MYH10, MYO15A, and MYO18A in HeLa cells (Fig. 3.20). Next, we explored whether the knockdown of these myosins affected the nuclear localization of 2P-MRLC. By downregulating MYH9, MYH10, MYO15A, and MYO18A expression using specific siRNAs (Fig. 3.21). , we assessed the nuclear presence of 2P-MRLC in knockdown (KD) and negative control (NC) cells on stiff glass substrates. Surprisingly, MYH9-KD cells exhibited an augmented nuclear localization of 2P-MRLC, whereas MYH10-KD cells showed a decreased nuclear presence of 2P-MRLC (Fig. 3.22). However, MYO15A-KD and MYO18A-KD did not alter the nuclear localization of 2P-MRLC (Fig. 3.22). Following these results, the presence or absence of nuclear MYH9 and MYH10 on the stiff substrate was confirmed by immunofluorescence staining. The results showed that MYH10 was present in the nucleus, while MYH9 could not be clearly identified in the nucleus (Fig. 3.23). These findings suggest that the substrate stiffness-driven nuclear translocation of 2P-

MRLC might be regulated by MYH9 and MYH10. Additionally, MYH10 might cooperate with 2P-MRLC in localizing to the nucleus in response to substrate stiffness.

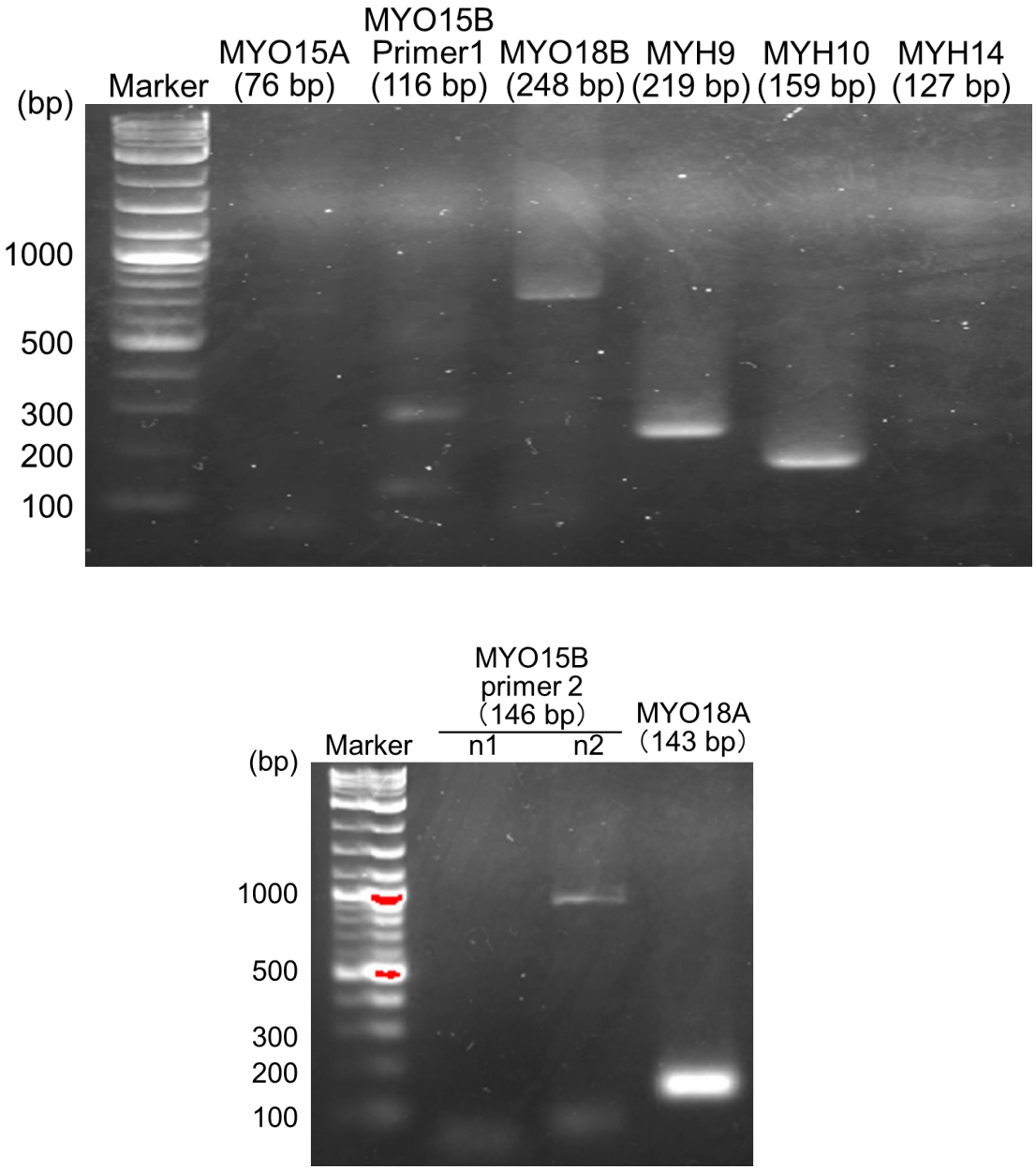

Fig. 3.20 Confirming myosin family expression in HeLa cells

The amplification of PCR using primers targeting the mRNA region of MYO15A, MYO15B, MYH9, MYH10, and MYH14 was conducted. Subsequently, the PCR products were separated using agarose gel electrophoresis.

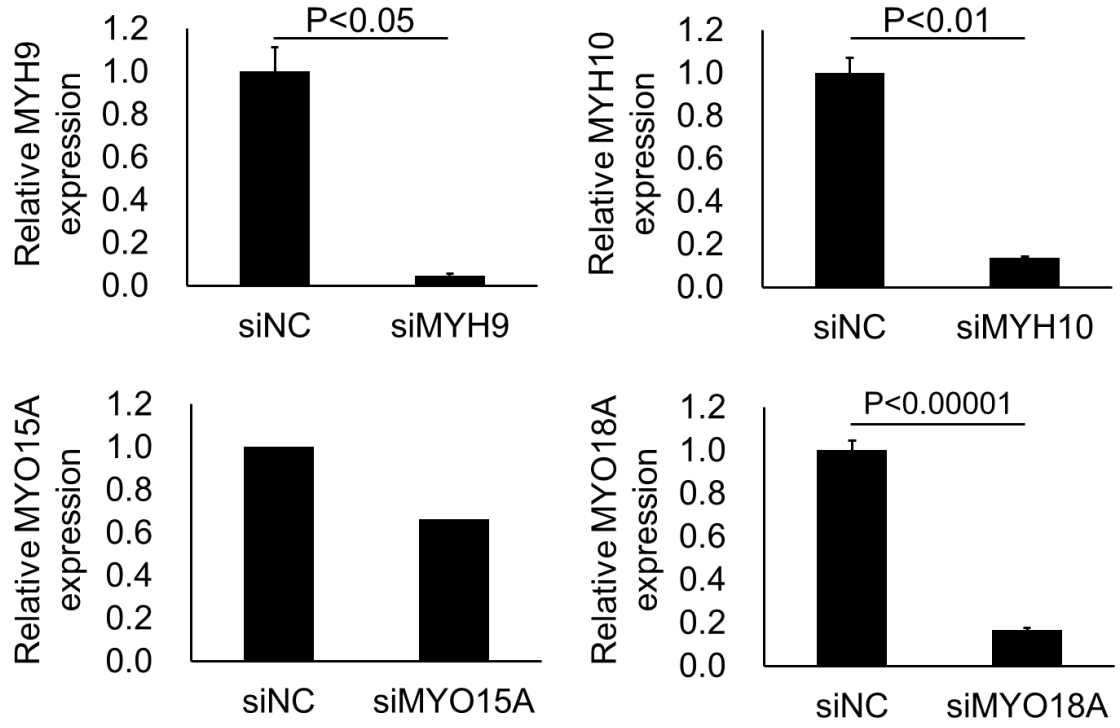

Fig. 3.21 Confirming knockdown efficiency of MYH9, MYH10, MYO15A and MYO18A.

The relative mRNA expression levels of MYH9, MYH10, MYO15A, and MYO18A were determined using qPCR in HeLa cells cultured on stiff plastic substrates following transfection with either the negative control of siRNA (siNC) or siRNA targeting MYH9, MYH10, MYO15A, and MYO18A (diMYH9, siMYH10, siMYO15A, and siMYO18A). This analysis was conducted across three independent experiments (MYO15A; one experiment). The bars in the graph represent the mean ± SEM

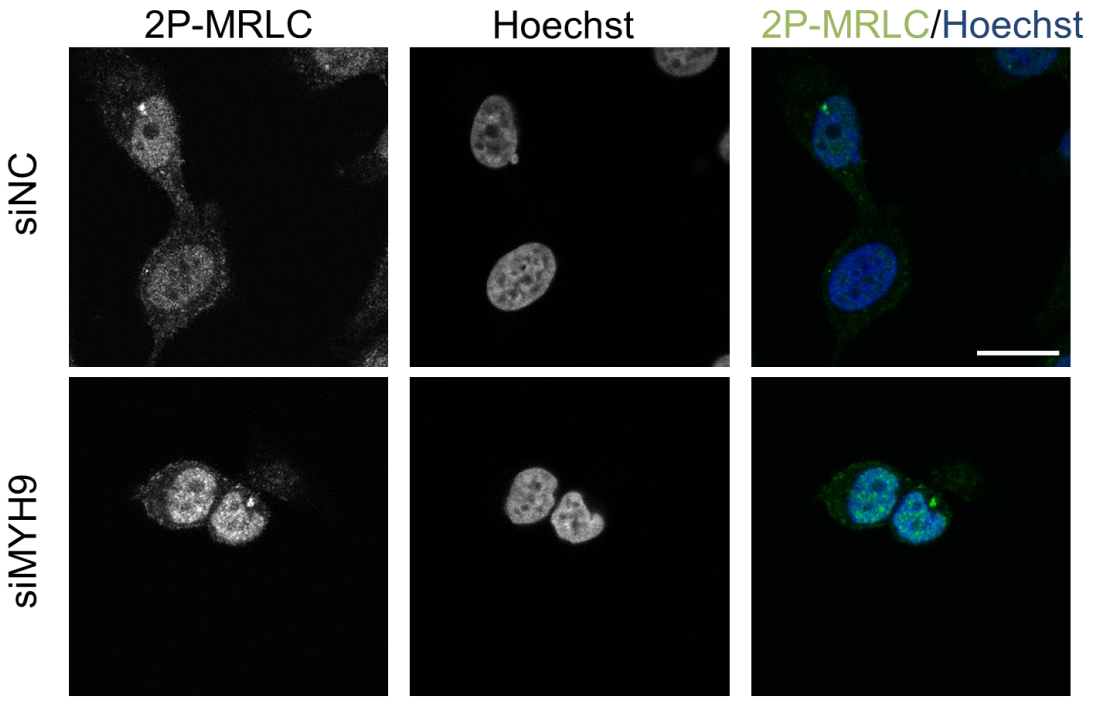
2P-MRLC
Hoechst
2P-MRLC/Hoechst
siNC
siMYH9

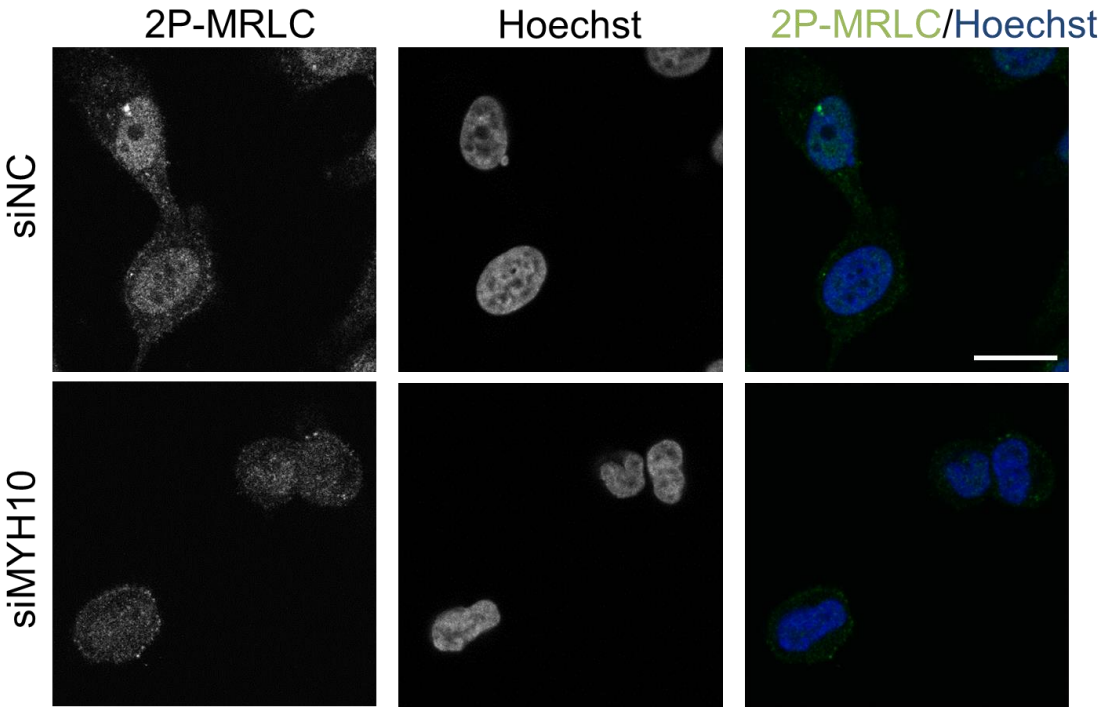
2P-MRLC
Hoechst
2P-MRLC/Hoechst
siNC
siMYH10

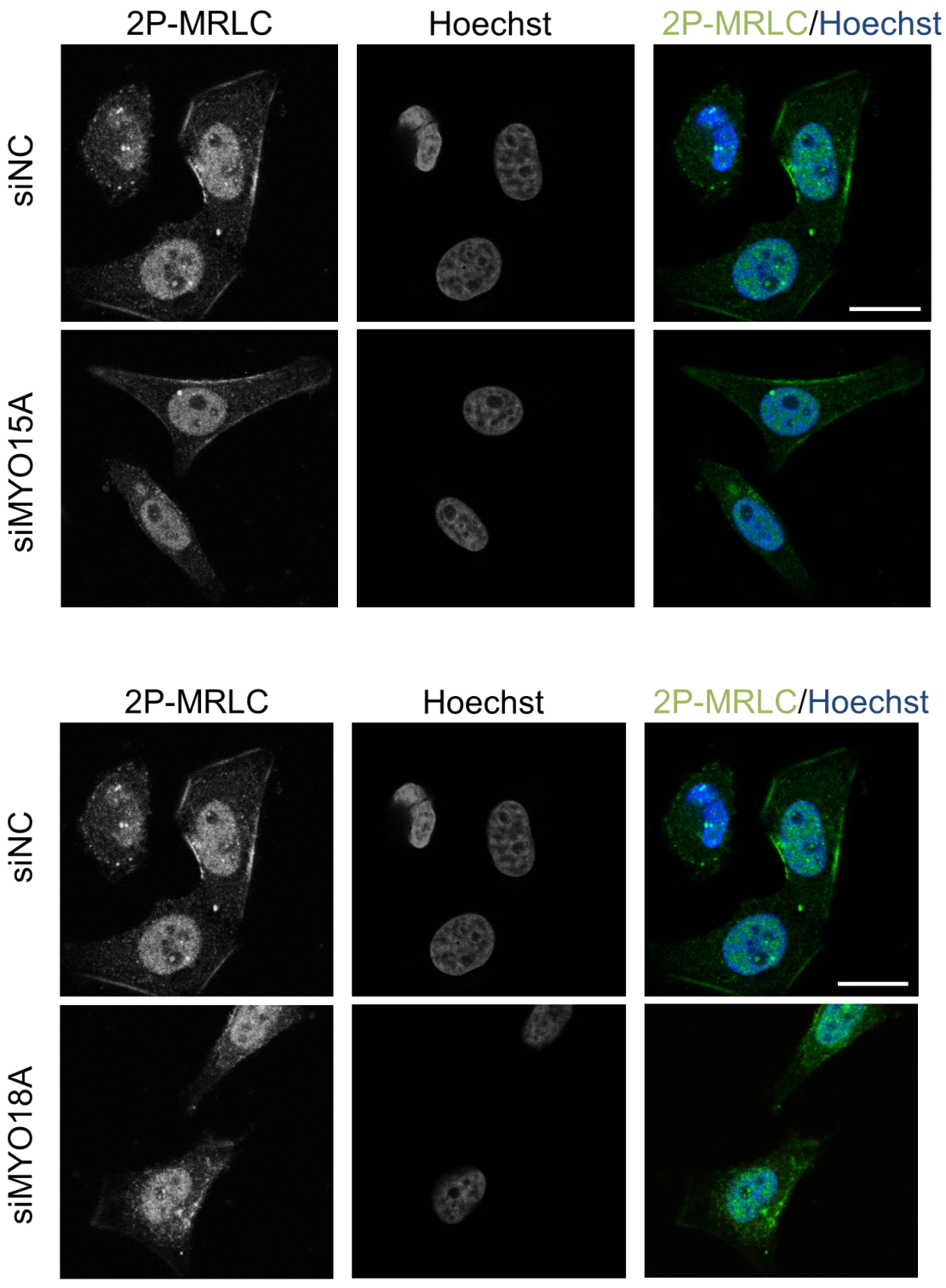

Fig. 3.22 Nuclear localization change of 2P-MRLC dependent on knockdown of MYH9, MYH10, MYO15A and MYO18A.

Illustrative immunofluorescent micrographs displaying 2P-MRLC and the nucleus observed in HeLa

cells on stiff glass substrates coated with collagen-I subsequent to transfection with either the negative control of short interfering RNA (siRNA) (siNC) or siRNA targeting MYH9 (siMYH9), MYH10 (siMYH10), MYO15A (siMYO15A), and MYO18A (siMYO18A). The scale bars represent 20 μm. This depiction represents observations from a single experiment.

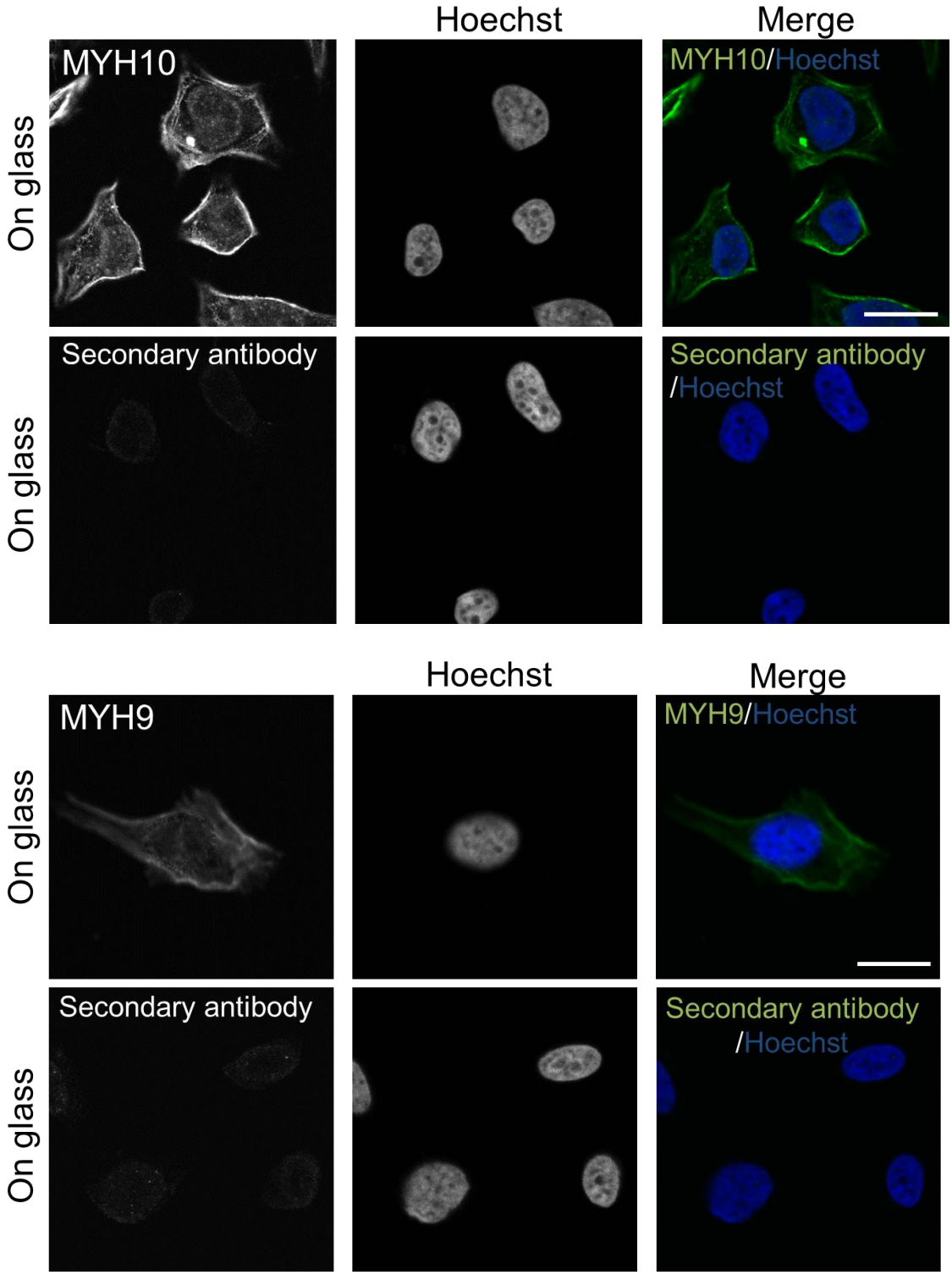

Fig. 3.23 Conforming the nuclear localization of MYH10 and MYH9

Exemplary immunofluorescent micrographs depicting MYH10 (or MYH9) and the secondary antibody observed in HeLa cells on glass substrates coated with collagen-I. Prior to

immunofluorescent staining, the cytosolic fraction was removed using a nuclear/cytosolic fractionation kit. This observation represents a single experiment. Scale bars represent 20 μm.

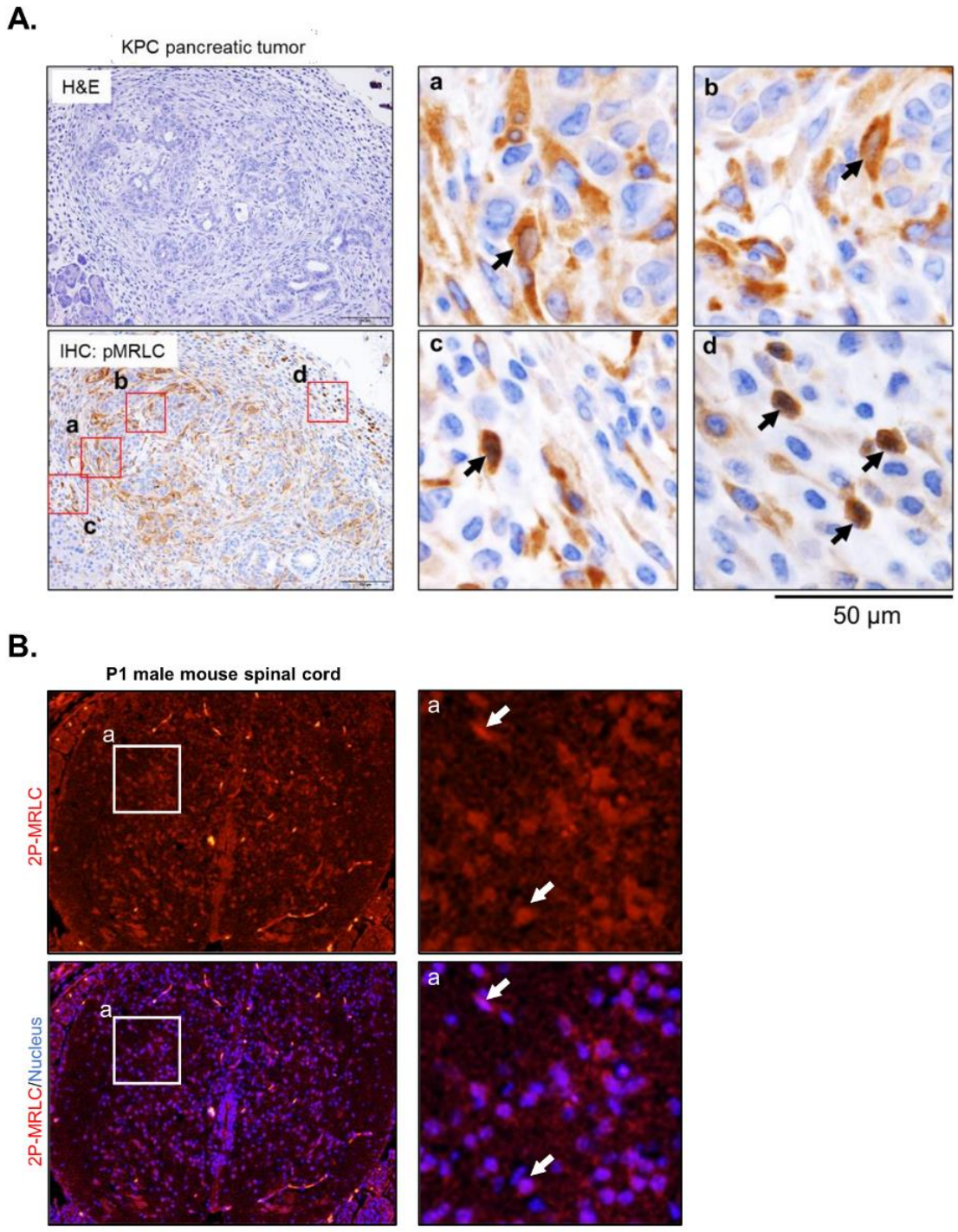

Fig. 3.24 Nuclear localization of 2P-MRLC in vivo

(A) Tissue sections extracted from pancreatic cancer developed in the KPC model underwent staining with hematoxylin and eosin (H&E, upper left panel) and 2P-MRLC (lower left panel).

The boxed regions (a–d) were further magnified in the adjacent panels. Arrows highlight cells exhibiting weak to moderate nuclear 2P-MRLC signals. (B) Immunohistochemical staining depicting 2P-MRLC in the spinal cord of a male P1 mouse. Arrows indicate cells displaying nuclear 2P-MRLC signals.

3-3 Discussion

We found that substrate stiffness play a pivotal role in promoting the nuclear presence of 2P-MRLC, a phenomenon tightly associated with ZIPK nuclear localization in response to the substrate's stiffness-triggered actin polymerization. While our study established the link between ZIPK and 2P-MRLC nuclear localization, the precise underlying mechanisms remain elusive.

Previous research has highlighted the significance of ZIPK dephosphorylation at T299 or inactivation of its LZ domain in facilitating nuclear translocation[32,33]. It's plausible that actin polymerization triggered by substrate stiffness could regulate these ZIPK modifications, subsequently promoting its nuclear localization. In terms of how ZIPK affects 2P-MRLC nuclear localization, while ZIPK possesses a nuclear localization sequence aiding its active transport into the nucleus[31], MRLC lacks such a sequence. There are possible scenarios: ZIPK might actively transport MRLC into the nucleus in response to substrate stiffness or MRLC could passively diffuse in. Studies indicate that smaller molecules (<40 kDa) can diffuse into HeLa cell nuclei[45], and substrate stiffness may facilitate such passive transport via nuclear stretching and pore opening[46]. Substrate stiffness may passively localize MRLC to the nucleus, followed by its phosphorylation by nuclear ZIPK.

We have shown by immunofluorescence staining that MYH10 is present in the nucleus on a stiff

substrate (Fig. 3.23). Furthermore, Knockdown of MYH10 also suppressed the nuclear localization of 2P-MRLC (*Fig. 3.22 Nuclear localization change of 2P-MRLC dependent on knockdown of MYH9, MYH10, MYO15A and MYO18A*.Fig. 3.22). Since MYH10 is a subunit of MRLC, it is possible that MYH10 also localizes to the nucleus with MRLC in a substrate stiffness-dependent manner.

Moreover, our analysis in the KPC mouse model showcased the presence of nuclear 2P-MRLC in tumor cells (Fig. S8A). We also revealed that nuclear 2P-MRLC suppressed MafB expression and apoptosis in response to stiffness. Given that pancreatic cancer exhibits increased tissue stiffness compared to normal pancreatic tissueand, and its association with aggressive phenotypes on stiff substrates[47,48]. Increased expression of lysyl oxidase-like 2, which promotes substrate stiffening, increases the number of 2P-MRLC-positive cells in pancreatic ductal adenocarcinoma[49]. This insight positions nuclear 2P-MRLC as a potential therapeutic target to counteract malignancy spurred by pancreatic tumor stiffening.

Of note, we found that 2P-MRLC existed in the nuclei of stromal cells in KPC mouse pancreatic tumors (Fig. S8A). Stromal cells, such as immune cells and fibroblasts, in the cancer microenvironment, which have recently attracted attention as targets for cancer therapy, have been

reported to respond to substrate stiffness[50]. Nuclear 2P-MRLC in these cells might indirectly influence cancer progression within the tumor microenvironment. This highlights the potential of targeting nuclear 2P-MRLC as a therapeutic approach to impede cancer progression driven by tumor stiffening.

Chapter 4

Nuclear localization of 2P-MRLC in response to substrate stiffness suppressed the MafB expression to repress apoptosis

4-1 Results

4-1-1 Nuclear localization of 2P-MRLC suppresses MafB expression

We aimed to unravel the functional implications of 2P-MRLC's nuclear localization provoked by substrate stiffness. Past studies have unveiled nuclear MRLC's role as a transcription factor in certain contexts, such as its binding to the CTNNB1 core promoter region in a gastric cancer cell line.[20,25,26]. To determine if 2P-MRLC exhibits similar binding characteristics in cells exposed to stiff substrates, we conducted ChIP-PCR assays. Remarkably, our findings revealed significant binding of 2P-MRLC to the CTNNB1 promoter region under such conditions (Fig. 4.1). These findings led us to speculate that nuclear 2P-MRLC might act as a transcriptional regulator, modulating specific gene expression in response to substrate stiffness. Consequently, we conducted comprehensive qPCR screenings to identify genes exhibiting at least a 1.15-fold alteration in expression under stiff substrate conditions (Fig. 4.2A). For these genes, we performed qPCR screening and explored the genes which is 1.15 times up- or downregulated by ZIPK activation (Fig. 4.2B). Finally, for these genes, we performed qPCR screening and explored genes which is 1.15 times up- or down-regulated by MRLC expression (Fig. 4.2C). Next, we confirmed whether the initial screening results were correct. First, to examine whether MRLC regulates MafB expression, we downregulated MRLC expression with specific siRNAs (Fig. 4.3A and B). This result showed MRLC-KD enhanced

MafB mRNA expression in HeLa, A431, A549, and MSC cells (Fig. 4.4). Next, we investigated MafB mRNA expression in HeLa cells on soft (0.4 kPa) or stiff (271 kPa) substrates. This result showed that MafB expression was suppressed on stiff substrates (Fig. 4.5). We also examined MafB mRNA expression in cells treated with a ZIPK inhibitor that suppressed the nuclear localization of 2P-MRLC. This result showed that the ZIPK inhibitor increased MafB expression (Fig. 4.6A). In addition, we confirmed that the inhibition of ZIPK promoted MafB protein expression by western blotting (Fig. 4.6B). These results indicate that the nuclear localization of 2P-MRLC triggered by ZIPK in response to substrate stiffness suppressed MafB expression.

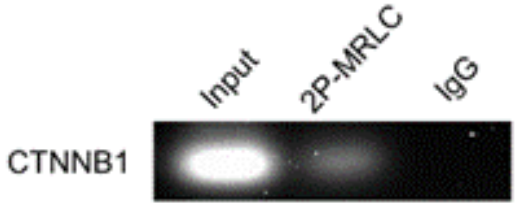

Fig. 4.1 Chromatin immunoprecipitation-polymerase chain reaction (ChIP-PCR) to assess 2P-MRLC bind to the CTNNB1 core promoter.

Primers targeting the core promoter region of catenin beta 1 (CTNNB1) were utilized for Chromatin Immunoprecipitation (ChIP) followed by Polymerase Chain Reaction (PCR) amplification. Subsequently, the PCR products were separated through agarose gel electrophoresis, demonstrating the binding of 2P-MRLC to the CTNNB1 core promoter. IgG was employed as a negative control.

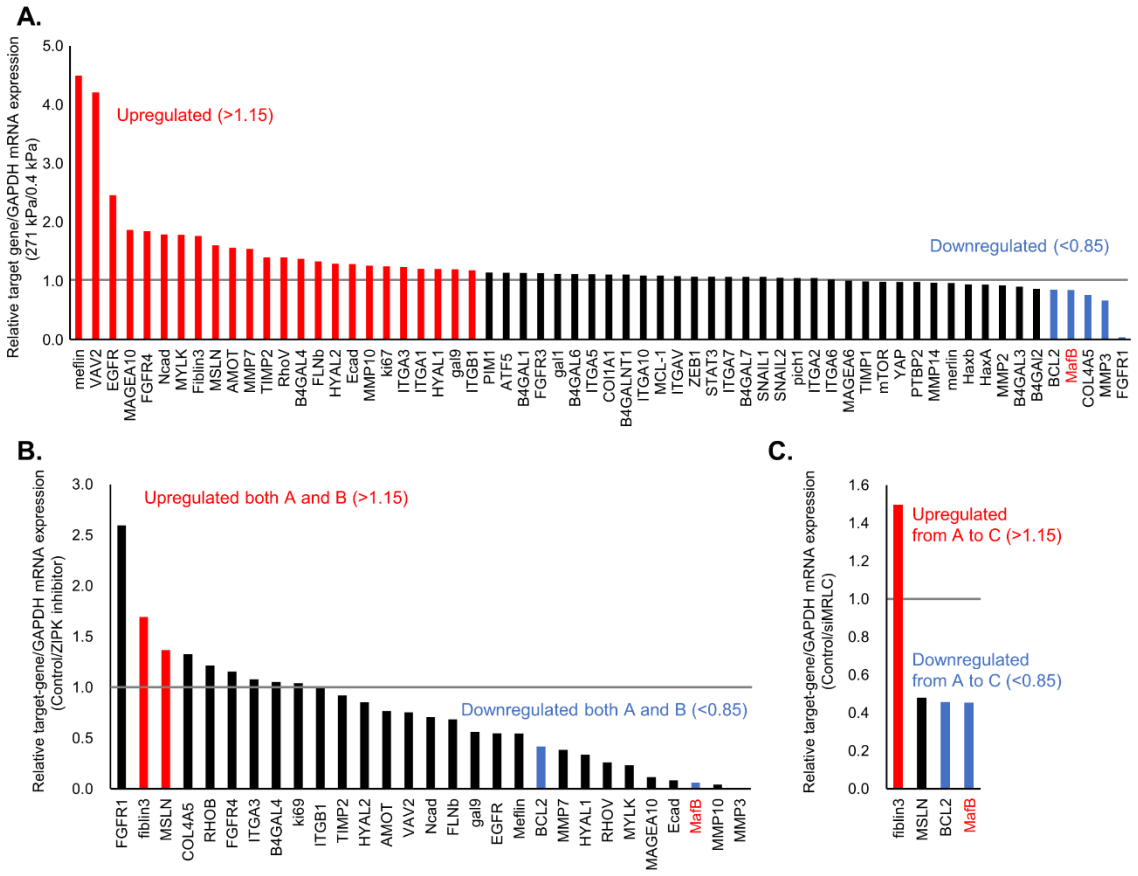

Fig. 4.2 First screening to determine the genes whose expression is regulated by nuclear 2P-MRLC.

(A–C) The relative mRNA expression of the target-gene/GAPDH in HeLa cells was assessed across different conditions: (A) on stiff (271 kPa) versus soft (0.4 kPa) polyacrylamide hydrogel substrates, (B) on stiff plastic substrates after treatment with dimethyl sulfoxide (DMSO) (control) versus ZIPK inhibitor, and (C) on stiff plastic substrates post-transfection with the negative control of siRNA (Control) versus siRNA targeting MRLC (siMRLC). These evaluations were conducted within a single experiment.

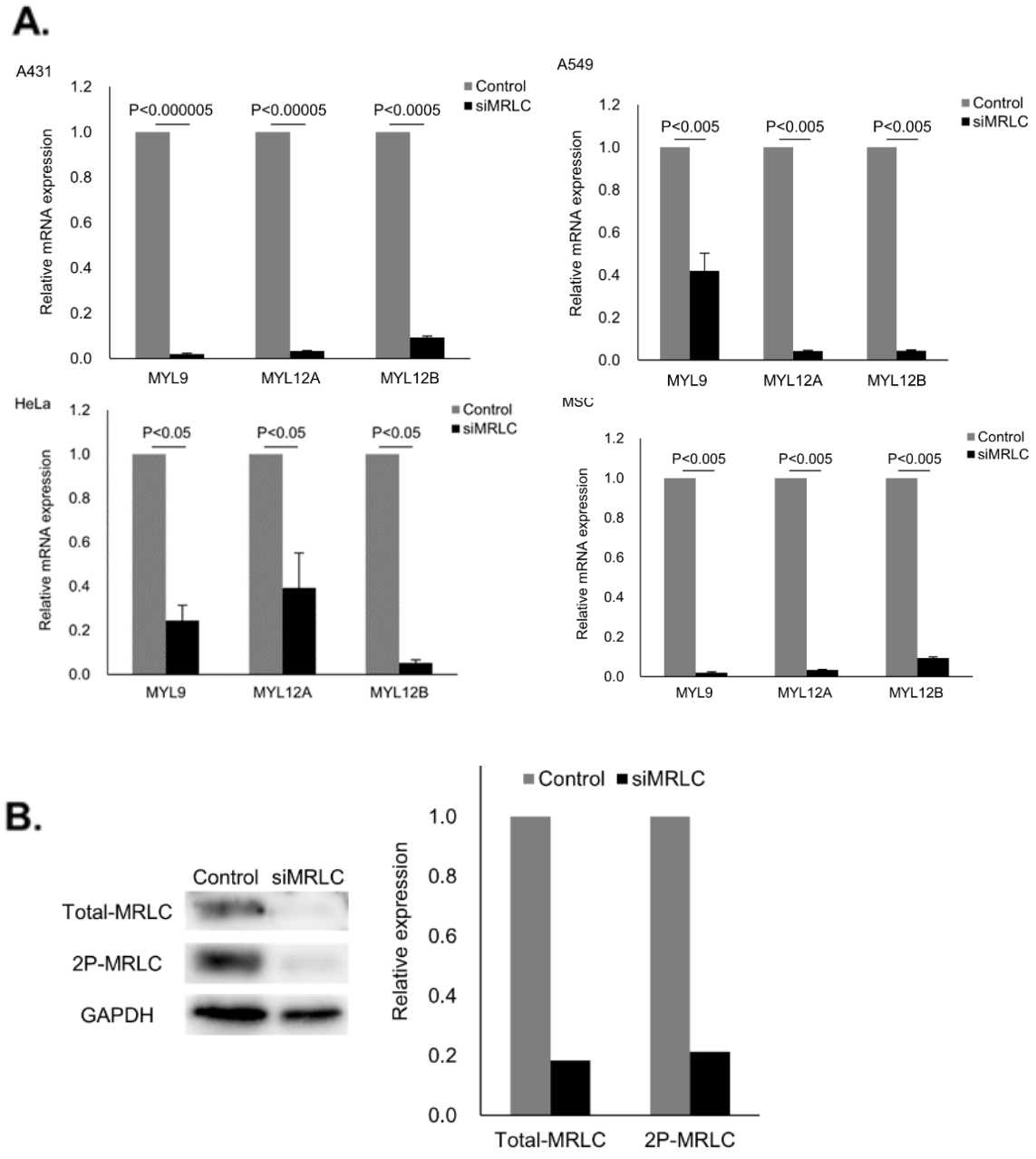

Fig. 4.3 Confirmation of knockdown efficiency with siRNA for MRLC

(A) The relative mRNA expression levels of MYL9, MYL12A, or MYL12B/GAPDH were determined via qPCR in A431 cells, A549 cells, HeLa cells, and MSCs subsequent to transfection with

either the negative control of siRNA (control) or siRNA targeting MRLC (siMRLC). (B) Western blot analysis (left) and quantification (right) of total-MRLC and 2P-MRLC levels in HeLa cells cultured on stiff plastic substrates post-transfection with either the negative control siRNA (control) or siRNA targeting MRLC (siMRLC). These evaluations were conducted within a single experiment.

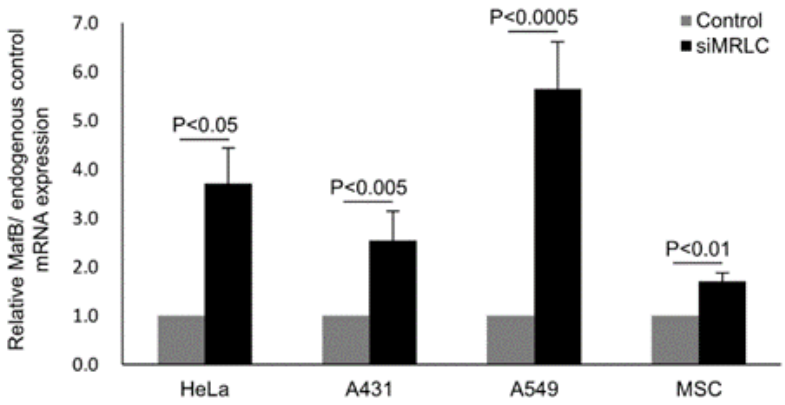

Fig. 4.4 MafB expression in MRLC knockdown condition.

The relative mRNA expression levels of MafB, normalized to endogenous control genes detected via quantitative PCR (qPCR), were assessed in HeLa cells, A431 cells, A549 cells, and mesenchymal stem cells (MSCs) cultivated on stiff plastic substrates following transfection with either the negative control of siRNA (control) or siRNA targeting MRLC (siMRLC). GAPDH was employed as the endogenous control gene in HeLa, A431, and A549 cells, while s18 served as the endogenous control in MSCs. These assessments were conducted across three independent experiments. The bars in the figures represent the mean ± SEM. Statistical significance was determined using an unpaired t-test.

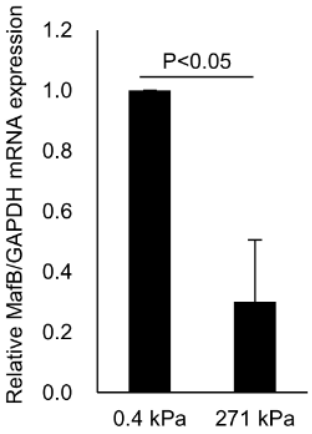

Fig. 4.5 MafB expression change in response to substrate stiffness.

The relative mRNA expression levels of MafB normalized to GAPDH were assessed via qPCR in HeLa cells cultured on either soft (0.4 kPa) or stiff (271 kPa) polyacrylamide hydrogel substrates. These assessments were conducted across three independent experiments. The bars in the figures represent the mean ± SEM. Statistical significance was determined using an unpaired t-test.

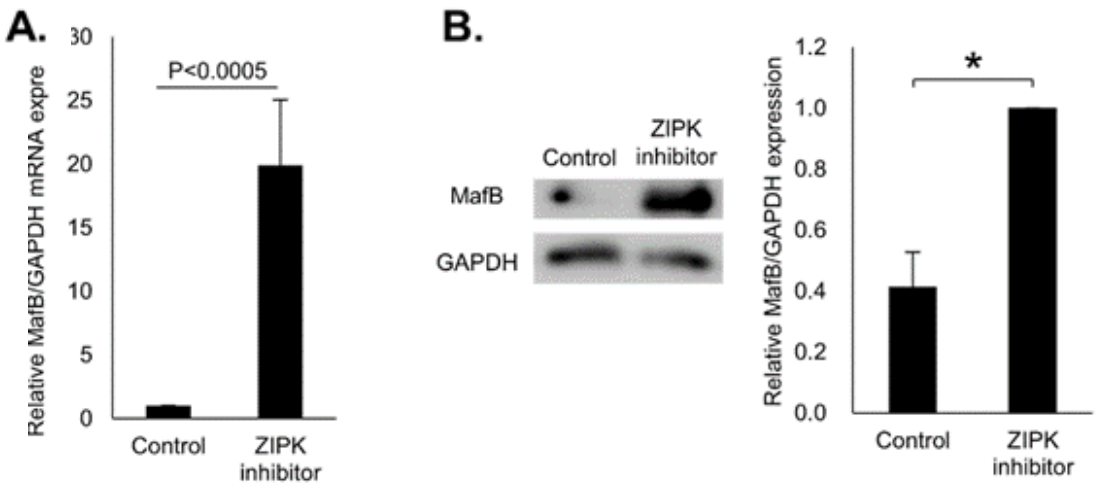

Fig. 4.6 MafB expression change by ZIPK inhibition.

(A) The relative mRNA expression levels of MafB normalized to GAPDH were determined via qPCR in HeLa cells cultured on stiff plastic substrates, post-treatment with or without ZIPK inhibitor. Statistical significance was assessed using an unpaired t-test. (B) Western blot analysis (left) and quantification (right) of MafB levels in HeLa cells cultured on stiff plastic substrates after treatment with DMSO (control) or ZIPK inhibitor. *Statistical significance was determined with a 95% confidence interval. These assessments were conducted across three independent experiments. The bars in the figures represent the mean ± SEM.

4-1-2 Nuclear localization of 2P-MRLC suppresses apoptosis via downregulation of MafB expression

Next, we examined the specific cellular response caused by the suppression of MafB expression mediated by nuclear 2P-MRLC in cells on stiff substrates. MafB promotes apoptosis during limb morphogenesis[51]. Thus, we hypothesized that suppression of MafB expression, which is induced by the nuclear localization of 2P-MRLC in response to substrate stiffness, prevents apoptosis. We first evaluated the cell death rates and levels of cleaved-caspase3, which is a typical apoptosis marker, in HeLa cells on stiff (0.4 kPa) or soft (271 kPa) substrates. The results showed that cells on stiff substrates exhibited reduced cell death rates and cleaved-caspase3 levels (Fig. 4.7A and B). Second, we examined the cell death rates and cleaved-caspase3 levels in NC, MRLC-KD, MRLC, and MafB double KD cells. The results showed that MRLC-KD cells exhibited increased cell death rates and cleaved-caspase3 levels, whereas MafB KD rescued this phenomenon in MRLC-KD cells (Fig. 4.8A and B). we also found that upregulation of apoptosis related genes in both the cells on soft substrate and MRLC knockdown cells by analyzing gene expression using DNA microarray (Fig. 4.9). Finally, we confirmed that MafB overexpression promoted cell death (Fig. 4.10). These results indicate that substrate stiffness drives the suppression of apoptosis via the downregulation of MafB expression and ZIPK-dependent nuclear localization of 2P-MRLC.

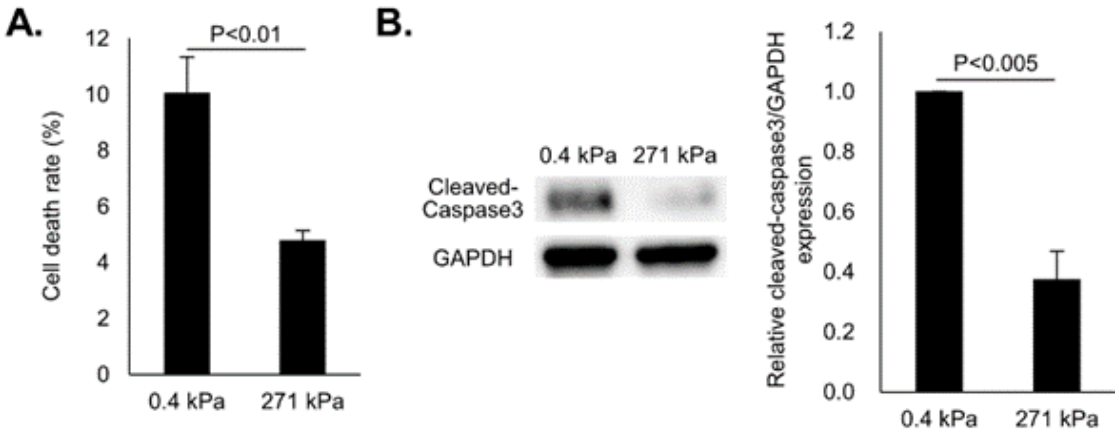

Fig. 4.7 Cell death rate and apoptosis regulated by substrate stiffness.

(A) Assessment of cell death rates via trypan blue staining in HeLa cells cultured on either soft (0.4 kPa) or stiff (271 kPa) substrates. (B) Evaluation of cleaved caspase3 levels through representative western blots (left) and subsequent quantification (right) in HeLa cells cultured on soft (0.4 kPa) or stiff (271 kPa) polyacrylamide hydrogel substrates. These experiments were conducted across three independent trials. The figures' bars denote the mean ± SEM. Statistical significance was determined using an unpaired t-test.

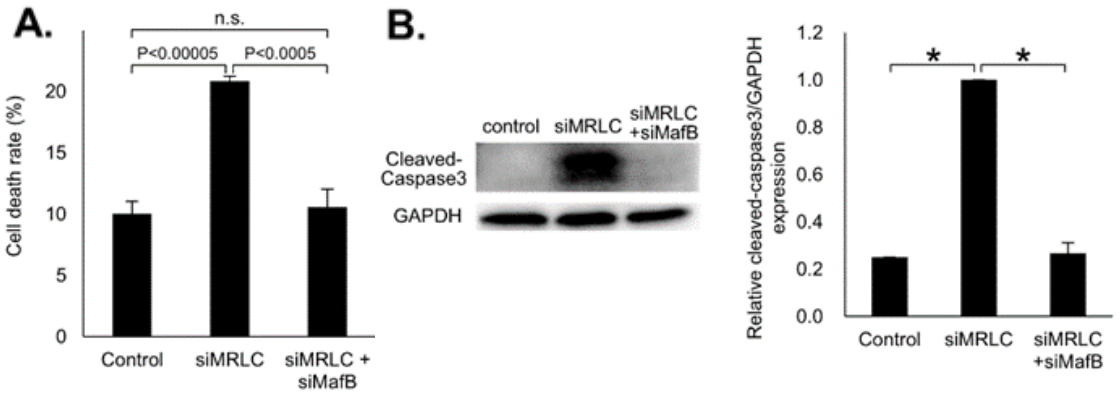

Fig. 4.8 Cell death rate and apoptosis in MRLC knockdown or MRLC and MafB double-knockdown condition.

(A) Cell death rate evaluated via trypan blue staining in HeLa cells on stiff plastic substrates after transfection with the negative control of siRNA (control), siRNA targeting MRLC (siMRLC), or (A) Assessment of cell death rates via trypan blue staining in HeLa cells cultured on either soft (0.4 kPa) or stiff (271 kPa) substrates. (B) Evaluation of cleaved caspase3 levels through representative western blots (left) and subsequent quantification (right) in HeLa cells cultured on soft (0.4 kPa) or stiff (271 kPa) polyacrylamide hydrogel substrates. These experiments were conducted across three independent trials. The figures' bars denote the mean ± SEM. Statistical significance was determined using an unpaired t-test.

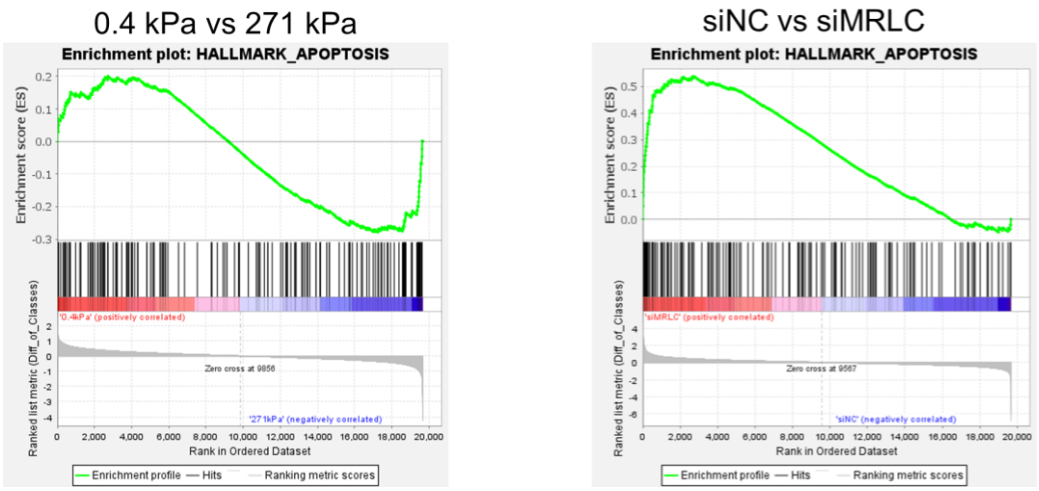

Fig. 4.9 Gene set enrichment analysis

GSEA showing apoptosis in the cells on soft substrate (A) and MRLC knockdown cells (B). FDR q value < 0.25.

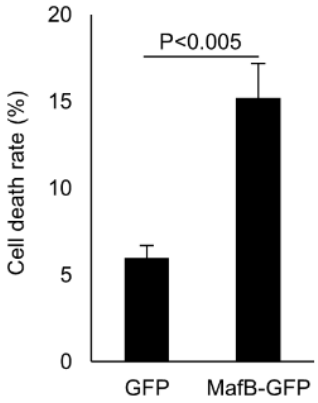

Fig. 4.10 Cell death rate in the condition of GFP or MafB-GFP overexpression.

The assessment of cell death rates was conducted via trypan blue staining in HeLa cells cultured on stiff plastic substrates subsequent to transfection with either GFP or MafB-GFP vectors. This evaluation was performed across four separate experiments. The bars in the figures represent the mean

± SEM. Statistical significance was determined using an unpaired t-test.

4-2-3 Low expression of MafB correlates with poor prognosis.

The correlation between MafB expression and the overall survival of patients with was examined based on the data of cervical and lung cell carcinoma present in the Kaplan Meier-plotter [52,53]. The low expression of MafB is correlated with a poor prognosis in cervical cancer patients and lung cancer patients (Fig. 4.11).

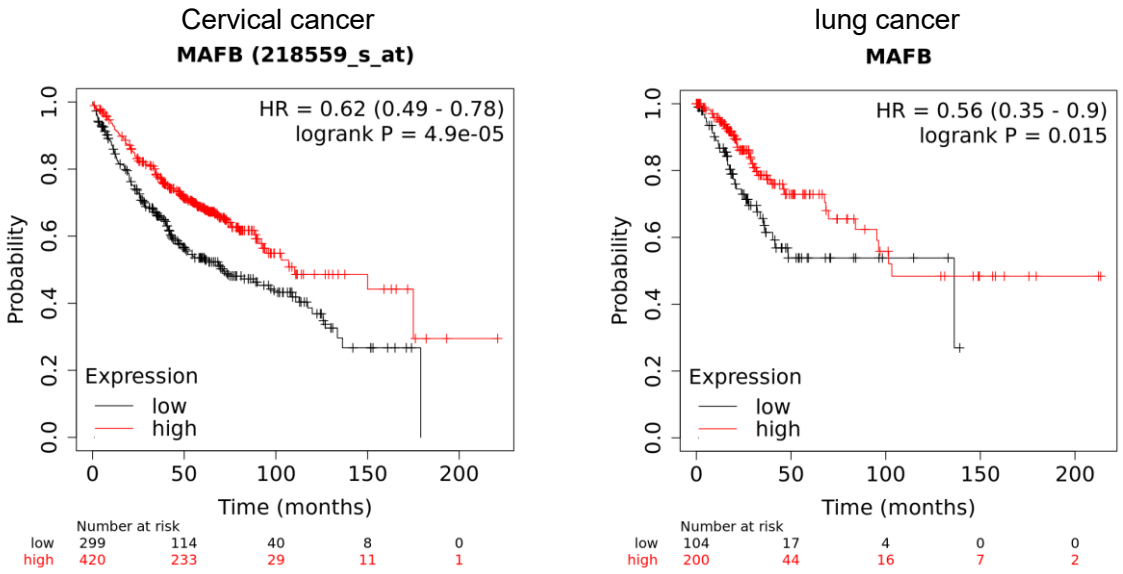

Fig. 4.11 Correlation MafB expression with poor prognosis in cervical cancer and lung cancer patients.

The high expression of MafB expression negatively correlates with the poor prognosis in cervical cancer patients (A) and lung cancer patients (B). Kaplan–Meier survival curves show the probability of overall survival. Red lines indicate patients with high expression of the gene and black lines indicate patients with low expression of the gene.

4-2 Discussion

Our investigation unveiled that the nuclear localization of 2P-MRLC led to the downregulation of MafB expression and concurrently suppressed apoptosis. This discovery introduces a fresh mechanism, demonstrating the regulation of apoptosis through the nuclear localization of 2P-MRLC, particularly influenced by substrate stiffness.

Our findings indicated the binding of 2P-MRLC to the CTNNB1 (β-catenin gene) promoter region specifically in cells residing on stiff substrates (Fig. 4.1). Previous reports have highlighted MRLC's binding to the CTNNB1 promoter, promoting CTNNB1 expression in gastric cancer cells[20]. Consequently, the interaction of 2P-MRLC with the CTNNB1 promoter region might elevate CTNNB1 expression levels. Past research has established that β-catenin activation due to substrate stiffness contributes to tumor growth and the intravasation of cancer cells[47,54]. 2P-MRLC potentially functions as an upstream regulatory factor governing substrate-stiffness-dependent β-catenin-mediated cancer malignancy.

Chapter 5

Summary and remaining question

Our results suggest a new mechanotransduction pathway mainly based on the nuclear localization of 2P-MRLC (Fig. 5.1).

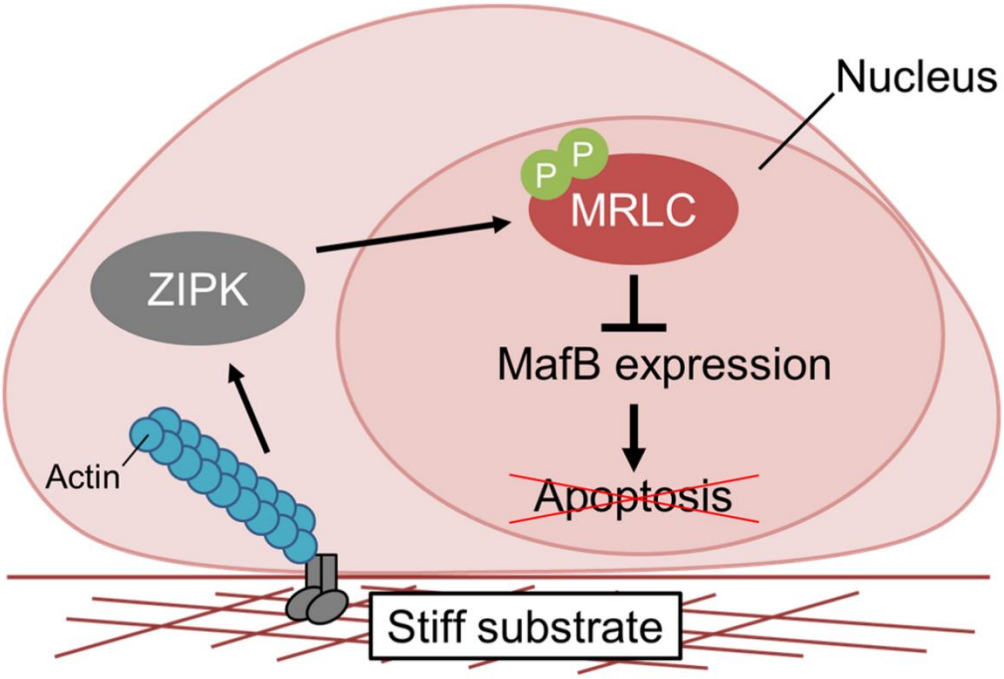

Fig. 5.1 Nuclear localization of 2P-MRLC in response to substrate stiffness suppresses apoptosis.

The nuclear localization of 2P-MRLC in response to substrate stiffness plays a role in suppressing apoptosis. Actin fiber formation, in response to substrate stiffness, triggers the activation of nuclear localization of 2P-MRLC through ZIPK. Consequently, the nuclear localization of 2P-MRLC downregulates MafB expression, further contributing to apoptosis suppression.

Our investigation elucidated that actin fiber formation, in response to substrate stiffness, is crucial for the nuclear localization of 2P-MRLC facilitated by ZIPK. Alterations in the direct interaction state

between actin and ZIPK or signaling pathways induced by actin polymerization may regulate ZIPK nuclear translocation, although the precise mechanisms remain unknown. Previous reports have highlighted the binding of Par-4 and RHOD to actin and ZIPK[55-57], suggesting their potential involvement in the nuclear localization of ZIPK triggered by substrate stiffness.

We also observed that MYH10 (non-muscle myosin 2) localizes in the nucleus on stiff substrates. Notably, knockdown of MYH10 suppressed the nuclear localization of 2P-MRLC, emphasizing the role of MYH10 as an essential subunit of MRLC. Thus, substrate stiffness facilitates the nuclear localization of MYH10 alongside 2P-MRLC. Previous studies have shown that MYH9, a member of the same myosin family as MYH10, binds to the promoter region of CTNNB1, regulating the transcription of this gene in conjunction with MRLC[20]. Further exploration is required to understand how substrate stiffness promotes the nuclear localization of MYH10. Previous studies have also reported that the Myosin family works with actin in the nucleus [58,59]. It has also been reported that the motor activity of myosin is necessary for the coordinated function of actin and myosin in the nucleus[60]. We have shown that the substrate stiffness-dependent double phosphorylation (ser18/Thr19) state of MRLC is localized in the nucleus. Since ser18/Thr19 phosphorylation induces myosin motor activity, substrate stiffness and nuclear localization of 2P-MRLC may be involved in the regulation of nuclear actin-myosin function in the nucleus.

We have indirectly observed that nuclear 2P-MRLC suppresses MafB expression. To confirm this effect, it is imperative to ascertain whether 2P-MRLC directly interacts with DNA regions involved in regulating MafB expression. This will be achieved through ChIP-seq analysis and ChIP-PCR techniques. Previous reports have indicated that MRLC interacts with an AGCTCC sequence[25]. Consequently, we have verified that the AGCTCC sequence is situated near the MafB coding region (Fig. 5.2). It is plausible that MRLC interacts with any of the regions depicted in Fig. 5.2.

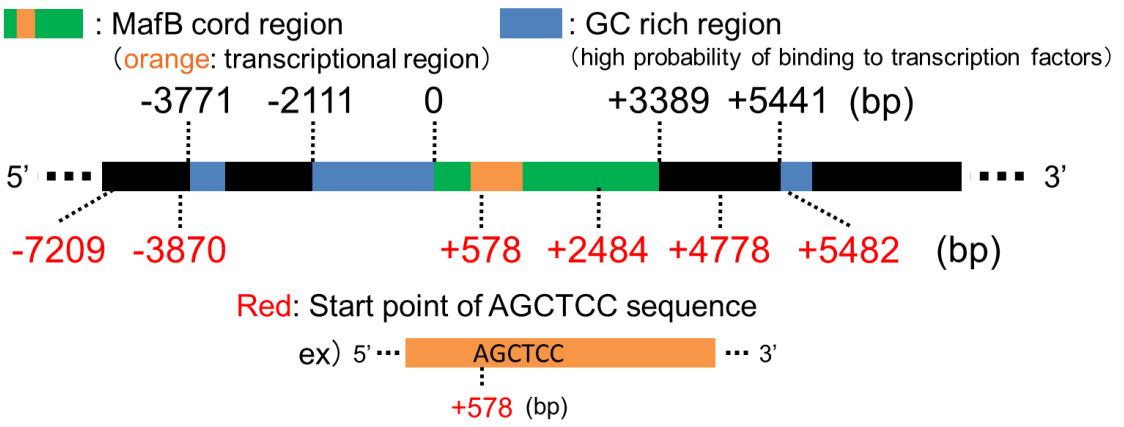

Fig. 5.2 Regions that MRLC may interact.

We have also shown that nuclear 2P-MRLC regulates apoptosis in MafB, but have not been able to elucidate its function beyond apoptosis. MafB has been reported to be involved in the regulation of keratinocyte differentiation[61], macrophage differentiation[62], M2 polarization of macrophage[63], male urethral formation[64]. We found that 2P-MRLC is expressed in the nucleus in immune cells of

KPC Pancreatic tumor (Fig. 3.23A). It has also been reported that mechanical stimuli are regulated in tumor stroma to control macrophage polarization[65]. Since macrophages are a type of immune cell, it is possible that 2P-MRLC regulates macrophage differentiation and polarization to M2 via MafB expression in the tumor stroma. It has also been reported that substrate stiffness regulates macrophage polarization[66]. Regarding the polarization of macrophages due to stiffness, both polarization toward M1[67-69] and polarization toward M2[70-72] have been reported. Stiffness-dependent nuclear localization of YAP has been reported to regulate macrophage polarization[67].This result suggests that nuclear 2P-MRLC may regulate MafB expression in immune cells in the tumor stroma. There is a report suggests that MafB is a marker for tumor-associated macrophages[73,74]. However, since polarization due to substrate stiffness is controlled by both M1 and M2, there may be polarization controls other than YAP. The effect of substrate stiffness-dependent nuclear localization of 2P-MRLC on macrophage polarization needs to be tested in the future.

We identified 2P-MRLC as a transcriptional regulator of apoptosis induced by soft substrates. Transcriptional regulators that control growth, differentiation, actin-mediated cell contraction, and cancer malignancy in a substrate stiffness-dependent manner have been identified[15,28,75,76], but factors that directly regulate apoptosis have not been found. Soft substrate-dependent increases in apoptosis have been reported in normal epithelial cells, breast cancer cell lines, porcine tubule-derived

cells, and rat annular cells[77-81]. It has been reported that the activity of caspase-3 by JNK activity[77], a kinase-active molecule, induces apoptosis, but the detailed mechanism has not yet been clarified. 2P-MRLC as a transcriptional regulatory molecule responsive to substrate stiffness that may directly regulate apoptosis.

In conclusion, our findings have revealed the substrate-stiffness-dependent nuclear localization of 2P-MRLC and a part of its localization mechanism. These findings provide new insights into the mechanism by which cells respond to substrate stiffening.

References

[1] Martino, F., Perestrelo, A.R., Vinarský, V., Pagliari, S. and Forte, G. (2018). Cellular Mechanotransduction: From Tension to Function. Front Physiol 9, 824.

[2] Pelham, R.J., Jr. and Wang, Y. (1997). Cell locomotion and focal adhesions are regulated by substrate flexibility. Proc Natl Acad Sci U S A 94, 13661-5.

[3] Smith, L., Cho, S. and Discher, D.E. (2017). Mechanosensing of matrix by stem cells: From matrix heterogeneity, contractility, and the nucleus in pore-migration to cardiogenesis and muscle stem cells in vivo. Semin Cell Dev Biol 71, 84-98.

[4] Smith, L.R., Cho, S. and Discher, D.E. (2018). Stem Cell Differentiation is Regulated by Extracellular Matrix Mechanics. Physiology (Bethesda) 33, 16-25.

[5] Barriga, E.H., Franze, K., Charras, G. and Mayor, R. (2018). Tissue stiffening coordinates morphogenesis by triggering collective cell migration in vivo. Nature 554, 523-527.

[6] Crest, J., Diz-Muñoz, A., Chen, D.Y., Fletcher, D.A. and Bilder, D. (2017). Organ sculpting by patterned extracellular matrix stiffness. Elife 6

[7] Lampi, M.C. and Reinhart-King, C.A. (2018). Targeting extracellular matrix stiffness to attenuate disease: From molecular mechanisms to clinical trials. Sci Transl Med 10

[8] Hui, L., Zhang, J., Ding, X., Guo, X. and Jiang, X. (2017). Matrix stiffness regulates the proliferation, stemness and chemoresistance of laryngeal squamous cancer cells. Int J Oncol 50, 1439-1447.

[9] Wei, S.C. et al. (2015). Matrix stiffness drives epithelial-mesenchymal transition and tumour metastasis through a TWIST1-G3BP2 mechanotransduction pathway. Nat Cell Biol 17, 678-88.

[10] Nia, H.T., Munn, L.L. and Jain, R.K. (2020). Physical traits of cancer. Science 370

[11] Dasgupta, I. and McCollum, D. (2019). Control of cellular responses to mechanical cues through YAP/TAZ regulation. J Biol Chem 294, 17693-17706.

[12] Du, J. et al. (2016). Extracellular matrix stiffness dictates Wnt expression through integrin pathway. Sci Rep 6, 20395.

[13] Shiwen, X. et al. (2015). A Role of Myocardin Related Transcription Factor-A (MRTF-A) in Scleroderma Related Fibrosis. PLoS One 10, e0126015.

[14] Zhang, K., Grither, W.R., Van Hove, S., Biswas, H., Ponik, S.M., Eliceiri, K.W., Keely, P.J. and Longmore, G.D. (2016). Mechanical signals regulate and activate SNAIL1 protein to control the fibrogenic response of cancer-associated fibroblasts. J Cell Sci 129, 1989-2002.

[15] Dupont, S. et al. (2011). Role of YAP/TAZ in mechanotransduction. Nature 474, 179-

83.

[16] Ishihara, S. and Haga, H. (2022). Matrix Stiffness Contributes to Cancer Progression by Regulating Transcription Factors. Cancers (Basel) 14

[17] Ishihara, S., Inman, D.R., Li, W.J., Ponik, S.M. and Keely, P.J. (2017). Mechano-Signal Transduction in Mesenchymal Stem Cells Induces Prosaposin Secretion to Drive the Proliferation of Breast Cancer Cells. Cancer Res 77, 6179-6189.

[18] Fischer, R.S., Myers, K.A., Gardel, M.L. and Waterman, C.M. (2012). Stiffness-controlled three-dimensional extracellular matrices for high-resolution imaging of cell behavior. Nat Protoc 7, 2056-66.

[19] Schneider, C.A., Rasband, W.S. and Eliceiri, K.W. (2012). NIH Image to ImageJ: 25 years of image analysis. Nat Methods 9, 671-5.

[20] Ye, G. et al. (2020). Nuclear MYH9-induced CTNNB1 transcription, targeted by staurosporin, promotes gastric cancer cell anoikis resistance and metastasis. Theranostics 10, 7545-7560.

[21] Iida, T. et al. (2022). Pharmacologic conversion of cancer-associated fibroblasts from a protumor phenotype to an antitumor phenotype improves the sensitivity of pancreatic cancer to chemotherapeutics. Oncogene 41, 2764-2777.

[22] Ikebe, M., Hartshorne, D.J. and Elzinga, M. (1986). Identification, phosphorylation, and dephosphorylation of a second site for myosin light chain kinase on the 20,000-dalton light chain of smooth muscle myosin. J Biol Chem 261, 36-9.

[23] Ikebe, M. (1989). Phosphorylation of a second site for myosin light chain kinase on platelet myosin. Biochemistry 28, 8750-5.

[24] Kondo, T., Okada, M., Kunihiro, K., Takahashi, M., Yaoita, Y., Hosoya, H. and Hamao, K. (2015). Characterization of myosin II regulatory light chain isoforms in HeLa cells. Cytoskeleton (Hoboken) 72, 609-20.

[25] Li, Q. and Sarna, S.K. (2009). Nuclear myosin II regulates the assembly of preinitiation complex for ICAM-1 gene transcription. Gastroenterology 137, 1051-60, 1060 e1-3.

[26] Zhang, Y.S. et al. (2015). A novel function of nuclear nonmuscle myosin regulatory light chain in promotion of xanthine oxidase transcription after myocardial ischemia/reperfusion. Free Radic Biol Med 83, 115-28.

[27] Zhang, Y.S. et al. (2018). Fasudil ameliorates the ischemia/reperfusion oxidative injury in rat hearts through suppression of myosin regulatory light chain/NADPH oxidase 2 pathway. Eur J Pharmacol 822, 1-12.

[28] Ishihara, S., Yasuda, M., Harada, I., Mizutani, T., Kawabata, K. and Haga, H. (2013). Substrate stiffness regulates temporary NF- κ B activation via actomyosin contractions. Exp Cell Res 319, 2916-27.

[29] Elbadawy, M., Usui, T., Yamawaki, H. and Sasaki, K. (2018). Novel Functions of Death-Associated Protein Kinases through Mitogen-Activated Protein Kinase-Related Signals. Int J Mol Sci 19

[30] Murata-Hori, M., Fukuta, Y., Ueda, K., Iwasaki, T. and Hosoya, H. (2001). HeLa ZIP kinase induces diphosphorylation of myosin II regulatory light chain and reorganization of actin filaments in nonmuscle cells. Oncogene 20, 8175-83.

[31] Shoval, Y., Pietrokovski, S. and Kimchi, A. (2007). ZIPK: a unique case of murine-specific divergence of a conserved vertebrate gene. PLoS Genet 3, 1884-93.

[32] Graves, P.R., Winkfield, K.M. and Haystead, T.A. (2005). Regulation of zipper-interacting protein kinase activity in vitro and in vivo by multisite phosphorylation. J Biol Chem 280, 9363-74.

[33] Weitzel, D.H., Chambers, J. and Haystead, T.A. (2011). Phosphorylation-dependent control of ZIPK nuclear import is species specific. Cell Signal 23, 297-303.

[34] Murata-Hori, M., Suizu, F., Iwasaki, T., Kikuchi, A. and Hosoya, H. (1999). ZIP kinase identified as a novel myosin regulatory light chain kinase in HeLa cells. FEBS Lett 451, 81-4.

[35] Okamoto, M., Takayama, K., Shimizu, T., Ishida, K., Takahashi, O. and Furuya, T. (2009). Identification of death-associated protein kinases inhibitors using structure-based virtual screening. J Med Chem 52, 7323-7.

[36] Mizutani, T., Haga, H., Koyama, Y., Takahashi, M. and Kawabata, K. (2006). Diphosphorylation of the myosin regulatory light chain enhances the tension acting on stress fibers in fibroblasts. J Cell Physiol 209, 726-31.

[37] Ikebe, M. and Hartshorne, D.J. (1985). Phosphorylation of smooth muscle myosin at two distinct sites by myosin light chain kinase. J Biol Chem 260, 10027-31.

[38] Ueda, K., Murata-Hori, M., Tatsuka, M. and Hosoya, H. (2002). Rho-kinase contributes to diphosphorylation of myosin II regulatory light chain in nonmuscle cells. Oncogene 21, 5852-60.

[39] Romet-Lemonne, G. and Jégou, A. (2013). Mechanotransduction down to individual actin filaments. Eur J Cell Biol 92, 333-8.

[40] Das, A., Fischer, R.S., Pan, D. and Waterman, C.M. (2016). YAP Nuclear Localization in the Absence of Cell-Cell Contact Is Mediated by a Filamentous Actin-dependent, Myosin II- and Phospho-YAP-independent Pathway during Extracellular Matrix Mechanosensing. J Biol Chem 291, 6096-110.

[41] Gavara, N., Sunyer, R., Roca-Cusachs, P., Farré, R., Rotger, M. and Navajas, D. (2006). Thrombin-induced contraction in alveolar epithelial cells probed by traction microscopy. J Appl Physiol (1985) 101, 512-20.

[42] Liu, Z., van Grunsven, L.A., Van Rossen, E., Schroyen, B., Timmermans, J.P., Geerts, A. and Reynaert, H. (2010). Blebbistatin inhibits contraction and accelerates migration in mouse hepatic stellate cells. Br J Pharmacol 159, 304-15.

[43] Heissler, S.M. and Sellers, J.R. (2014). Myosin light chains: Teaching old dogs new tricks. Bioarchitecture 4, 169-88.

[44] Woolner, S. and Bement, W.M. (2009). Unconventional myosins acting unconventionally. Trends Cell Biol 19, 245-52.

[45] Samudram, A., Mangalassery, B.M., Kowshik, M., Patincharath, N. and Varier, G.K. (2016). Passive permeability and effective pore size of HeLa cell nuclear membranes. Cell Biol Int 40, 991-8.

[46] Elosegui-Artola, A. et al. (2017). Force Triggers YAP Nuclear Entry by Regulating Transport across Nuclear Pores. Cell 171, 1397-1410.e14.

[47] Reid, S.E. et al. (2017). Tumor matrix stiffness promotes metastatic cancer cell interaction with the endothelium. EMBO J 36, 2373-2389.

[48] Rice, A.J., Cortes, E., Lachowski, D., Cheung, B.C.H., Karim, S.A., Morton, J.P. and Del Río Hernández, A. (2017). Matrix stiffness induces epithelial-mesenchymal transition and promotes chemoresistance in pancreatic cancer cells. Oncogenesis 6, e352.

[49] Alonso-Nocelo, M. et al. (2022). Macrophages direct cancer cells through a LOXL2-mediated metastatic cascade in pancreatic ductal adenocarcinoma. Gut

[50] Wei, J., Yao, J., Yan, M., Xie, Y., Liu, P., Mao, Y. and Li, X. (2022). The role of matrix stiffness in cancer stromal cell fate and targeting therapeutic strategies. Acta Biomater 150, 34-47.

[51] Suda, N. et al. (2014). Dimeric combinations of MafB, cFos and cJun control the apoptosis-survival balance in limb morphogenesis. Development 141, 2885-94.

[52] Győrffy, B. (2023). Discovery and ranking of the most robust prognostic biomarkers in serous ovarian cancer. Geroscience

[53] Lánczky, A. and Győrffy, B. (2021). Web-Based Survival Analysis Tool Tailored for Medical Research (KMplot): Development and Implementation. J Med Internet Res 23, e27633.

[54] Samuel, M.S. et al. (2011). Actomyosin-mediated cellular tension drives increased tissue stiffness and β-catenin activation to induce epidermal hyperplasia and tumor growth. Cancer Cell 19, 776-91.

[55] Vetterkind, S., Illenberger, S., Kubicek, J., Boosen, M., Appel, S., Naim, H.Y., Scheidtmann, K.H. and Preuss, U. (2005). Binding of Par-4 to the actin cytoskeleton is essential for Par-4/Dlk-mediated apoptosis. Exp Cell Res 305, 392-408.

[56] Gad, A.K., Nehru, V., Ruusala, A. and Aspenström, P. (2012). RhoD regulates

cytoskeletal dynamics via the actin nucleation-promoting factor WASp homologue associated with actin Golgi membranes and microtubules. Mol Biol Cell 23, 4807-19.

[57] Nehru, V., Almeida, F.N. and Aspenström, P. (2013). Interaction of RhoD and ZIP kinase modulates actin filament assembly and focal adhesion dynamics. Biochem Biophys Res Commun 433, 163-9.

[58] de Lanerolle, P. (2012). Nuclear actin and myosins at a glance. J Cell Sci 125, 4945-9.

[59] Caridi, C.P. et al. (2018). Nuclear F-actin and myosins drive relocalization of heterochromatic breaks. Nature 559, 54-60.

[60] Cook, A.W., Gough, R.E. and Toseland, C.P. (2020) Nuclear myosins - roles for molecular transporters and anchors. In J Cell Sci ed.^eds). © 2020. Published by The Company of Biologists Ltd., England.

[61] Miyai, M. et al. (2016) Transcription Factor MafB Coordinates Epidermal Keratinocyte Differentiation. In J Invest Dermatol ed.^eds), pp. 1848-1857. © 2016 The Authors. Published by Elsevier Inc, United States.

[62] Hamada, M., Tsunakawa, Y., Jeon, H., Yadav, M.K. and Takahashi, S. (2020). Role of MafB in macrophages. Exp Anim 69, 1-10.

[63] Kim, H. (2017). The transcription factor MafB promotes anti-inflammatory M2 polarization and cholesterol efflux in macrophages. Sci Rep 7, 7591.

[64] Matsushita, S. et al. (2018) Regulation of masculinization: androgen signalling for external genitalia development. In Nat Rev Urol ed.^eds), pp. 358-368, England.

[65] Hoffmann, E.J. and Ponik, S.M. (2020). Biomechanical Contributions to Macrophage Activation in the Tumor Microenvironment. Front Oncol 10, 787.

[66] Adams, S., Wuescher, L.M., Worth, R. and Yildirim-Ayan, E. (2019). Mechano-Immunomodulation: Mechanoresponsive Changes in Macrophage Activity and Polarization. Ann Biomed Eng 47, 2213-2231.

[67] Meli, V.S. et al. (2020). YAP-mediated mechanotransduction tunes the macrophage inflammatory response. Sci Adv 6

[68] Dutta, B., Goswami, R. and Rahaman, S.O. (2020). TRPV4 Plays a Role in Matrix Stiffness-Induced Macrophage Polarization. Front Immunol 11, 570195.

[69] Okamoto, T., Takagi, Y., Kawamoto, E., Park, E.J., Usuda, H., Wada, K. and Shimaoka, M. (2018) Reduced substrate stiffness promotes M2-like macrophage activation and enhances peroxisome proliferator-activated receptor γ expression. In Exp Cell Res ed.^eds), pp. 264-273. © 2018 Elsevier Inc, United States.

[70] Chuang, Y.C., Chang, H.M., Li, C.Y., Cui, Y., Lee, C.L. and Chen, C.S. (2020). Reactive Oxygen Species and Inflammatory Responses of Macrophages to Substrates with Physiological Stiffness. ACS Appl Mater Interfaces 12, 48432-48441.

[71] Pergola, C. et al. (2017). Modulation of actin dynamics as potential macrophage subtype-targeting anti-tumour strategy. Sci Rep 7, 41434.

[72] Xing, X. et al. (2021). Matrix stiffness-mediated effects on macrophages polarization and their LOXL2 expression. FEBS J 288, 3465-3477.

[73] Yadav, M.K. et al. (2020) Transcription factor MafB is a marker of tumor-associated macrophages in both mouse and humans. In Biochem Biophys Res Commun ed.^eds), pp. 590-595. © 2019 Elsevier Inc, United States.

[74] Samir, O., Kobayashi, N., Nishino, T., Siyam, M., Yadav, M.K., Inoue, Y., Takahashi, S. and Hamada, M. (2022). Transcription Factor MAFB as a Prognostic Biomarker for the Lung Adenocarcinoma. Int J Mol Sci 23

[75] Virdi, J.K. and Pethe, P. (2021). Biomaterials Regulate Mechanosensors YAP/TAZ in Stem Cell Growth and Differentiation. Tissue Eng Regen Med 18, 199-215.

[76] Nukuda, A., Sasaki, C., Ishihara, S., Mizutani, T., Nakamura, K., Ayabe, T., Kawabata, K. and Haga, H. (2015). Stiff substrates increase YAP-signaling-mediated matrix metalloproteinase-7 expression. Oncogenesis 4, e165.

[77] Chen, Y. et al. (2021) Protective autophagy attenuates soft substrate-induced apoptosis through ROS/JNK signaling pathway in breast cancer cells. In Free Radic Biol Med ed.^eds), pp. 590-603. © 2021 Elsevier Inc, United States.

[78] Chiu, W.T., Wang, Y.H., Tang, M.J. and Shen, M.R. (2007). Soft substrate induces apoptosis by the disturbance of Ca2+ homeostasis in renal epithelial LLC-PK1 cells. J Cell Physiol 212, 401-10.

[79] Zhang, Y.H., Zhao, C.Q., Jiang, L.S. and Dai, L.Y. (2011) Substrate stiffness regulates apoptosis and the mRNA expression of extracellular matrix regulatory genes in the rat annular cells. In Matrix Biol ed.^eds), pp. 135-44. © 2010 International Society of Matrix Biology. Published by Elsevier B.V, Netherlands.

[80] Chiu, W.T., Tang, M.J., Jao, H.C. and Shen, M.R. (2008). Soft substrate up-regulates the interaction of STIM1 with store-operated Ca2+ channels that lead to normal epithelial cell apoptosis. Mol Biol Cell 19, 2220-30.

[81] Kocgozlu, L. et al. (2010) Selective and uncoupled role of substrate elasticity in the regulation of replication and transcription in epithelial cells. In J Cell Sci ed.^eds), pp. 29-39, England.

Acknowledgment

First, I would like to thank Prof. Hisashi Haga for your critical guidance on my research. I also appreciate for giving me research environment and discretion to realize my ideas. I learned the joy of pursue one thing thoroughly.

I appreciate Dr. Seiichiro Ishihara for kind and helpful support. I learned how to write a research paper and how to present research from you. You have been grown me as a researcher.

I would like to express my gratitude to Prof. Tomoyasu Aizawa and Prof. Ryota Uehara. All discussion with you helped me to improve my presentation in doctoral defense and this dissertation.

Thanks to the past/current members of Laboratory of Cell Dynamics. The time I spent with you all is a precious treasure for me. Thanks for the happy memories.

Finally, I would like to express my sincere gratitude to my family for the continuous support. They helped me a lot financially and mentally and always respected and encouraged me. I want to contribute to your future happier life from now on.